

# Statistical Properties of Collisionless Equal- and Unequal-Mass Merger Remnants of Disk Galaxies

Thorsten Naab

*Institute of Astronomy, Cambridge University, Madingley Road, Cambridge, CB3 0HA*

*Max-Planck-Institut für Astronomie, Königstuhl 17, 69117 Heidelberg*

Andreas Burkert

*Max-Planck-Institut für Astronomie, Königstuhl 17, 69117 Heidelberg*

## ABSTRACT

We perform a large parameter survey of collisionless N-body simulations of binary mergers of disk-galaxies with mass ratios of 1:1, 2:1, 3:1, and 4:1 using the special purpose hardware GRAPE. A set of 112 merger simulations is used to investigate the fundamental statistical properties of merger remnants as a function of the initial orientation and the mass ratio of the progenitor disks. The photometric and kinematical properties of the simulated merger remnants are analyzed. The methods used to determine the characteristic properties are equivalent to the methods used for observations of giant elliptical galaxies. We take projection effects into account and analyze the remnant properties in a statistical way for comparison with observations. The basic properties of the remnants correlate with the mass ratio of the progenitor disks. We find that about 80% of the equal-mass merger simulations lead to slowly rotating merger remnants having  $(v/\sigma)^* < 0.4$ . Observers would interpret those objects as being supported by anisotropic velocity dispersions. All 1:1 remnants show significant minor-axis rotation. One half of all projected 1:1 remnants shows boxy ( $a_4 < 0$ ) and the other half shows disk ( $a_4 > 0$ ) isophotes. A distinct subclass of 4 out of 12 initial orientations leads to purely boxy remnants independent of orientation. 1:1 mergers with other initial orientations show disk or boxy isophotes depending on the viewing angle. Remnants with mass ratios of 3:1 and 4:1 have more homogeneous properties. They all rotate fast (maximum value of  $(v/\sigma) = 1.2$ ) and show a small amount of minor-axis rotation, consistent with models of isotropic or slightly anisotropic oblate rotators. If observed in projection they would be

interpreted as being supported by rotation. About 90% of the projected 3:1 and 4:1 remnants show disk isophotes. 2:1 remnants show intermediate properties. Projection effects lead to a large spread in the data in good agreement with observations. They do not change the fundamental kinematical differences between equal-mass and unequal-mass merger remnants. The correlation between isophotal twist and apparent ellipticity of every single merger remnant is in good agreement with observations. The amount of twisting strongly depends on the orientation of the remnant but is only weakly dependent on the mass ratio of the merger. The results of this study weaken the disk merger scenario as the possible formation mechanism of massive boxy giant ellipticals as only equal-mass mergers with special initial orientations can produce purely boxy anisotropic merger remnants. Some orientations of 1:1 mergers can even lead to disk and anisotropic remnants which are either not observed or would be classified as S0s based on their morphology. In general, the properties of equal-mass (and 2:1) merger remnants are consistent with the observed population of giant ellipticals in the intermediate mass regime between low mass fast rotating disk and bright massive boxy giant ellipticals. 3:1 and 4:1 merger remnants, however, are in very good agreement with the class of low luminosity, fast rotating giant elliptical galaxies. Binary mergers of disk galaxies are therefore still very good candidates for being the main formation mechanism for intermediate and low mass giant ellipticals. The homogeneous class of massive boxy ellipticals most likely formed by a different process.

*Subject headings:* galaxies: interaction – galaxies: structure – galaxies: evolution – galaxies: ellipticals – methods: numerical

## 1. Introduction

Detailed observations of individual giant elliptical galaxies have shown that they can be subdivided into two groups with respect to their structural properties (Bender, Döbereiner & Möllenhoff 1988; Bender 1988; Kormendy & Bender 1996) [BDM, and references therein]. Faint giant ellipticals are isotropic rotators with small minor axis rotation and disk deviations of their isophotal contours from perfect ellipses. They might contain faint disks which contribute up to 30% to the total light in the galaxy. Therefore their disk-to-bulge ratios overlap with those of S0-galaxies (Rix & White 1990; Scorza & Bender 1995). Disk ellipticals have power-law inner density profiles (Lauer et al. 1995; Faber et al. 1997) and show little or no radio and X-ray emission (Bender et al. 1989). Boxy ellipticals, on the other

hand, are in general more massive than disk ellipticals. They have box-shaped isophotes, and show flat cores. The kinematics of boxy ellipticals is generally more complex than that of disk ellipticals. They rotate slowly, are supposed to be supported by velocity anisotropy and have a large amount of minor axis rotation. A number of rotationally supported ellipticals also show boxy isophotes. These systems are either purely boxy (this is supposed to originate from tidal interactions with nearby massive companions) or show disk isophotes in the inner part and boxy isophotes in the outer part (Nieto & Bender 1989). Occasionally, boxy ellipticals have kinematically distinct cores (Franx & Illingworth 1988; Jedrzejewski & Schechter 1988; Bender 1988). These cores inhabit flattened rapidly rotating disk- or torus-like components dominating the light in the central few hundred parsecs (Bender 1990; Rix & White 1992; Mehlert et al. 1998), but they contribute only a few percent to the total light of the galaxy. The fact that these cores are metal-enhanced shows that gas (at least in the inner regions) must have played an important role during their formation (Bender & Surma 1992; Davies, Sadler & Peletier 1993; Bender 1996; Davies 1996). Boxy ellipticals show stronger radio emission than the average and have high X-ray luminosities consistent with emission from hot gaseous halos (Beuing et al. 1999). The distinct physical properties of disk and boxy elliptical galaxies point to the fact that both types of ellipticals could have different formation histories. It has been argued by Kormendy & Bender (1996) and Faber et al. (1997) that the observed stellar disks and the high density power law centers in disk ellipticals are signatures of dissipation during their formation. In this sense they seem to continue the Hubble sequence from S0s to higher bulge-to-disk ratios (Kormendy & Bender 1996). Boxy ellipticals with an even higher bulge-to-disk ratio show a stronger kinematical decoupling at their centers and no signature of a disk at all. Therefore the early type Hubble sequence from S0s to massive ellipticals might represent galaxies with a disk component embedded in more prominent spheroidal body.

The traditional view on the formation and evolution of giant elliptical galaxies is that they are very old stellar systems and formed very early at a redshift of more than two (Searle, Sargent & Bagnuolo 1973). After an intensive initial star-formation phase they experienced very little mass evolution (Bruzual & Charlot 1993). It has been argued by many authors that the stellar evolution of ellipticals is compatible with pure passive evolution models (Bower, Lucey & Ellis 1992; Aragon-Salamanca et al. 1993; Bender, Ziegler & Bruzual 1996; Ellis et al. 1997; Ziegler & Bender 1997) or models with exponentially decaying star formation (Ziegler et al. 1999). Alternatively, hierarchical theories of galaxy formation predict that massive galaxies were assembled relatively late in many generations of mergers of disk-type galaxies or smaller subunits and mass accretion. It has been argued by Kauffmann (1996) and Kauffmann & Charlot (1998) that this merger scenario is consistent with observations of

galaxies at different redshifts. The idea that elliptical galaxies can form from mergers of disk-galaxies has been originally proposed by Toomre & Toomre (1972). Thereafter the “merger hypothesis“ has been investigated in great details by many authors. For a recent review of current models of spheroid formation see Burkert & Naab (2003a,b). Negroponte & White (1983), Barnes (1988) and Hernquist (1992) performed the first fully self-consistent merger models of two equal-mass stellar disks embedded in dark matter halos. The remnants were slowly rotating, pressure supported and anisotropic systems and generally followed an  $r^{1/4}$  surface density profile in the outer parts. However, due to phase space limitations (Carlberg 1986) it was necessary to start with progenitors with massive central bulge components (Hernquist 1993b) to fit the observed de Vaucouleurs profile also in the inner parts. These simulations showed that global properties of equal-mass merger remnants resemble those of ordinary slowly rotating massive elliptical galaxies. More detailed investigations of isophotal shapes of the merger remnants have shown that the same remnant can appear either disky or boxy when viewed from different directions (Hernquist 1993b) with a trend pointing to boxy isophotes (Heyl Hernquist & Spergel 1994; Steinmetz & Buchner 1955). Barnes (1998) and Bendo & Barnes (2000) investigated a sample of disk-disk mergers with a mass ratio of 3:1 and found that the remnants are flattened and fast rotating in contrast to equal-mass mergers. Naab, Burkert & Hernquist (1999) investigated the photometric and kinematical properties of a prototypical 3:1 merger remnant in details and compared the results to observational data of disky elliptical galaxies. They found an excellent agreement and proposed that fast rotating disky elliptical galaxies can originate from pure collisionless 3:1 mergers while slowly rotating, pressure supported ellipticals form from equal-mass mergers of disk galaxies. In this paper we extend the analysis of Naab, Burkert & Hernquist (1999). A large number of 112 merger remnants resulting from a statistically unbiased sample of simulations of mergers between disk-galaxies with mass ratios of 1:1, 2:1, 3:1, and 4:1 is investigated. This large sample allows a much more thorough investigation of the statistical properties of merger remnants as all previous studies. After a short description of the simulation methods in section 2 we investigate the photometric and kinematic properties of the simulated remnants in section 3. We discuss the drawback of our results on the theory of the formation of elliptical galaxies in section 4.

## 2. The merger models

The spiral galaxies were constructed in dynamical equilibrium using the method described by Hernquist (1993). We used the following system of units: gravitational constant  $G=1$ , exponential scale length of the larger disk  $h = 1$  and mass of the larger disk  $M_d = 1$ . Each galaxy consists of an exponential disk, a spherical, non-rotating bulge with

mass  $M_b = 1/3$ , a Hernquist density profile (Hernquist 1990) with a scale length  $r_b = 0.2h$  and a spherical pseudo-isothermal halo with a mass  $M_d = 5.8$ , cut-off radius  $r_c = 10h$  and core radius  $\gamma = 1h$ .

We followed a sequence of mass ratios of the progenitor disks from  $\eta = 1$  to  $\eta = 4$  where  $\eta$  is the mass of the more massive galaxy divided by the mass of the merger partner. The equal-mass mergers were calculated adopting in total 400000 particles with each galaxy consisting of 20000 bulge particles, 60000 disk particles, and 120000 halo particles. We decided to use twice as many halo particles than disk particles to reduce heating and instability effects in the disk components (Naab, Burkert & Hernquist 1999). For the mergers with  $\eta = 2, 3, 4$  the parameters of the more massive galaxy were as described above. The low-mass companion contained a fraction of  $1/\eta$  the mass and the number of particles in each component with a disk scale length of  $h = \sqrt{1/\eta}$ , as expected from the Tully-Fisher relation (Pierce & Tully 1992).

The N-body simulations for the equal-mass mergers were performed by direct summation of the forces using the special purpose hardware GRAPE6 (Makino, Fukushige & Namura 2003). With this highly efficient hardware one force calculation for 400000 particles takes approx. 11 seconds. The mergers with mass ratios  $\eta = 2, 3, 4$  were followed using the newly developed treecode VINE (Wetzstein et al., 2003) in combination with the GRAPE5 (Kawai, Fukushige, Makino, & Taiji 2000) hardware for which the code was optimized. VINE uses a binary tree in combination with the refined multipole acceptance criterion proposed by Warren & Salmon (1995). This criterion takes the mass distribution of every node into account. It enables the user to control the absolute force error which is introduced by the tree construction. We chose a value of 0.001 which guarantees that the error resulting from the tree is smaller than the intrinsic force error of the GRAPE5 hardware which is of the order of 0.1%. To compensate for the limited mass resolution of GRAPE5 we limit the maximum mass of a tree node to  $10^3$  times the minimum particle mass. To further increase the speed of the calculation we only use GRAPE5 if forces for more than 50 particles are needed at the same time. Otherwise we compute the forces on the host computer as for small particle numbers the communication time between the board and the host computer exceeds the time for the force calculation on the host. With the parameters given above one force calculation with VINE and GRAPE5 for 400000 particles takes approx. 12 seconds.

We used a gravitational Plummer-softening of  $\epsilon = 0.05$  and a fixed leap-frog integration time step of  $\Delta t = 0.04$ . For the equal-mass mergers simulated with direct summation on GRAPE6 the total energy is conserved, VINE in combination with GRAPE5 conserves the total energy up to 0.5%.

The galaxies approached each other on nearly parabolic orbits with an initial separation

of  $r_{sep} = 30$  length units and a pericenter distance of  $r_p = 2$  length units (same parameters as e.g. Hernquist (1992)). A study of orbits of merging dark matter halos in cosmological large scale simulations by Khochfar (2003) has shown that most of the merging halos are indeed on parabolic orbits. The inclinations of the two disks relative to the orbit plane were  $i_1$  and  $i_2$  with arguments of pericenter  $\omega_1$  and  $\omega_2$ . In selecting unbiased initial parameters for the disk inclinations we followed the procedure described by Barnes (1998). For the spin vector of each disk we defined four different orientations pointing to every vertex of a regular tetrahedron. The initial orientations we used translate to the following set of angles: For the first galaxy  $i_1 = (0, -109, -109, -109)$ ,  $\omega_1 = (0, -60, 180, 60)$ . The second galaxy has  $i_2 = (180, 71, 71, 71)$ ,  $\omega_2 = (0, -30, 30, 90)$ . These parameters result in 16 initial configurations for equal-mass mergers and 16 more for every mass ratio  $\eta = 2, 3, 4$  where the initial orientations are interchanged. Following the simple hypothesis that the orientations of the merging disks are independent of each other and independent of their mutual orbital plane, every merger geometry has an equal probability to be realized (Barnes 1998). The orbital parameters are listed in Table 1. In total we simulated 112 mergers. The total computing time for the entire sample was about 1600 hours wall clock time.

For all simulations the merger remnants were allowed to settle into equilibrium approximately 8 to 10 dynamical times after the merger was complete. Then their equilibrium state was analyzed.

### 3. Photometric and kinematical properties of the remnants

To compare our simulated merger remnants with observations we analyzed the remnants with respect to observed global photometric and kinematical properties of giant elliptical galaxies, e.g. surface density profiles, isophotal deviation from perfect ellipses, velocity dispersion, and major- and minor-axis rotation. Defining characteristic values for each projected remnant we followed as closely as possible the analysis described by BDM.

#### 3.1. Isophotal shape

An artificial image of the remnant was created by binning the central 10 length units into  $128 \times 128$  pixels. This picture was smoothed with a Gaussian filter of standard deviation 1.5 pixels. The isophotes and their deviations from perfect ellipses were then determined using a data reduction package kindly provided by Ralf Bender.

To be confident that a once determined isophotal shape is characteristic for the remnant

and does not change with time we investigated the time evolution of the ellipticity and the  $a_4$  profile starting  $\approx 20$  time units after the merger of the bulge components was complete and followed the evolution for the next 50 time units. In intervals of four time units the luminous part of the remnant was transformed to the principal axes of its moment of inertia tensor. The tensor was evaluated using 40% of the most tightly bound particles. The isophotal properties were then analyzed as seen along the minor axis

The characteristic ellipticity  $\epsilon_{\text{eff}}$  for each projection was defined as the isophotal ellipticity at  $1.5r_e$ . Figure 1 shows the ellipticity profiles for the 3:1 merger remnant 10 in intervals of four time units starting at  $t = 150$ . The ellipticity profile shows little evolution with time and so does  $\epsilon_{\text{eff}}$  (small box). The behaviour of this simulation is characteristic for the whole set of simulations.

Following the definition of BDM for the global properties of observed giant elliptical galaxies, we determined for every projection the effective  $a_4$ -coefficient,  $a4_{\text{eff}}$ , as the mean value of  $a_4$  between  $0.25r_e$  and  $1.0r_e$ , with  $r_e$  being the projected spherical half-mass radius. In case of a strong peak in the  $a_4$ -distribution with an absolute value that is larger than the absolute mean value, we chose the peak value. Being characteristic for all merger remnants Figure 2 shows the  $a_4$ -profiles at different times for the 3:1 merger remnant with geometry 10. Figure 3 shows the corresponding  $a_4$ -profiles for the equal-mass remnant with geometry 2. Although the individual  $a_4$ -profiles differ in details at different time steps the global characteristic shape is conserved. This is reflected in the time evolution of  $a4_{\text{eff}}$  which was assigned to each remnant at the different time steps as shown in the small diagrams of Figure 2 and Figure 3. The change in  $a4_{\text{eff}}$  due to evolutionary effects (a real change in the isophotal shape and/or a change in three-dimensional shape leading to a different projection angle) is of the same order as the error due to the limited particle number. The bootstrap error bar is shown in the small diagrams of Figure 1 and Figure 2.

These measurements convinced us that the photometric properties of the inner regions (inside one effective radius) of the merger remnants evolve relatively fast into an equilibrium configuration. As the photometric properties do not significantly change with time they can be used for a further statistical analysis.

To investigate projection effects we determined for each simulation  $a4_{\text{eff}}$  and  $\epsilon_{\text{eff}}$  for 500 random projections of every remnant. This resulted in 8000 projections for  $\eta = 1$  and 16000 projections for  $\eta = 2, 3, 4$ , respectively.

The normalized histograms of projected ellipticities are shown in Figure 4. For equal-mass mergers the distribution rises from a small number of projections with zero ellipticity

to a peak around  $\epsilon_{\text{eff}} = 0.3$  and then falls to zero at  $\epsilon_{\text{eff}} = 0.7$ . 2:1 remnants show one peak around  $\epsilon_{\text{eff}} = 0.25$  and a strong peak at  $\epsilon_{\text{eff}} = 0.45$  falling to zero at  $\epsilon_{\text{eff}} = 0.7$ . 3:1 and 4:1 remnants show a flat distribution for small ellipticities rising to a strong peak around  $\epsilon_{\text{eff}} = 0.55$  and  $\epsilon_{\text{eff}} = 0.6$ , respectively. No projection leads to ellipticities larger than 0.7.

The distribution function for the isophotal shapes of equal-mass remnants peaks at  $a4_{\text{eff}} \approx -0.5$  and declines rapidly for more negative values (Figure 5). In total 47% of the projected 1:1 remnants show disk-like isophotes distributed in a broader wing for positive  $a4_{\text{eff}}$ . For higher mass ratios the distribution functions have a similar shape but are shifted to more positive values of  $a4_{\text{eff}}$ . 2:1 remnants peak at around  $a4_{\text{eff}} = 0.5$  and 73% of the projected remnants show disk-like isophotes. The distributions for 3:1 and 4:1 remnants both peak around  $a4_{\text{eff}} \approx 1$ . For these systems the fraction of disk-like projections is about 89% and 91%, respectively.

In addition, the 500 projected values for  $a4_{\text{eff}}$  and  $\epsilon_{\text{eff}}$  were used to calculate the two-dimensional probability density function for a given simulated remnant to be "observed" in the  $a4_{\text{eff}}-\epsilon_{\text{eff}}$  plane. We added up the probability densities assuming equal weights for every simulation geometry at a given mass ratio. Figure 6 shows the results for mergers with  $\eta = 1, 2, 3$ , and 4. The contours indicate the areas of 50% (dashed line), 70% (thin line) and 90% (thick line) probability to detect a merger remnant with the given properties. Observed data points from BDM are over-plotted. Filled boxes are boxy ellipticals with  $a4_{\text{eff}} \leq 0$  while open diamonds indicate disk-like ellipticals with  $a4_{\text{eff}} > 0$ . The errors were estimated applying the statistical bootstrapping method (Heyl Hernquist & Spergel 1994). The area covered by 1:1 remnants with negative  $a4_{\text{eff}}$  is in good agreement with the observed data for boxy elliptical galaxies. In particular the observed trend for more boxy galaxies to have higher ellipticities is reproduced. The disk-like equal-mass remnants also follow the trend for observed disk-like ellipticals. Remnants with an  $a4_{\text{eff}}$  around zero can have slightly higher ellipticities than observed. Remnants with  $\eta = 2, 3$ , and 4 predominantly populate the region of disk-like ellipticals and more disk-like ellipticals also tend to be more flattened. There is a trend for projections with  $a4_{\text{eff}} \approx 1$  to have slightly higher ellipticities than observed (or at a given ellipticity the remnants are not disk-like enough). Observed very disk-like ellipticals with relatively small ellipticities can not be reproduced.

In summary there is a clear trend for unequal-mass mergers to produce more disk-like remnants. Responsible for the disk-like appearance of the 3:1 and 4:1 remnants is the distribution of the particles of the massive disk. Figure 7 shows the different contributions from the small and the large progenitor galaxy and the resulting isophotal map of a characteristic 3:1 merger remnant. The particles originating from the small progenitor accumulate in a torus-like structure that has peanut-shaped or boxy isophotes. In contrast, the dominant



luminous material from the larger progenitor still keeps its disk-like appearance. In combination, the contribution from the larger progenitor – since it is three times more massive – dominates the overall properties of the remnant. This result holds for all 3:1 and 4:1 merger remnants. The more massive disk component is not completely destroyed during the merger event and determines the overall structure of the remnant. For equal-mass mergers both disks are affected during the merger and they can lose the memory of their initial state.

The isophotal analysis also provides information about the radial change of the relative orientation of the major axes of the isophotes. In general, the amount of isophotal twist depends on the projection angle. This is demonstrated in Figure 8 for a more elongated and a nearly round projection of a 3:1 merger remnant. To get a quantitative measure for the isophotal twist we determined the relative position angle  $\Delta\Phi$  between the isophote at  $0.5 r_{\text{eff}}$  and  $1.5 r_{\text{eff}}$  for every projection of the remnant. Figure 9 shows a comparison of isophotal twists for characteristic remnants with  $\eta = 1, 2, 3,$  and  $4$ . The isophotal twist is in general larger for projections that appear nearly round. For ellipticities larger than  $\epsilon_{\text{eff}} \approx 0.4$  the isophotal twist is  $\Delta\Phi \leq 20^\circ$ . The distribution of  $\Delta\Phi$  versus  $\epsilon_{\text{eff}}$  for random projections of every remnant is consistent with observations of elliptical galaxies (Bender, Döbereiner & Möllenhoff 1988). However, the simulated remnants can show larger isophotal twists at high ellipticities than observed galaxies. In addition there seems to exist no obvious correlation between the mass ratio of the galaxies and the amount of isophotal twist.

### 3.2. Kinematics

The central velocity dispersion  $\sigma_0$  of every remnant was determined as the average projected velocity dispersion of the luminous particles inside a projected galactocentric distance of  $0.2r_e$ . We defined the characteristic rotational velocity along the major and the minor axis as the projected rotational velocity at  $1.5r_e$  and  $0.5r_e$ , respectively. Figure 10 shows the time evolution for these velocity measurements for a 3:1 merger simulation which is characteristic for all simulations. The derived kinematical properties of the remnants stay nearly constant over a long time period and are therefore a good measurement of the intrinsic kinematics of the simulated remnants. Again, the bootstrap error is of the same order as the change of the measured values with time.

Like for the isophotal shape we computed the statistical kinematical properties of the simulated remnants and compared them with observational data of elliptical galaxies.

The normalized histograms for  $(v_{\text{maj}}/\sigma_0)$  are shown in Figure 11.

There is a clear trend for 1:1 mergers to produce slowly rotating ellipticals with  $(v_{\text{maj}}/\sigma_0) <$

0.3. For 2:1 mergers the peak value is around  $(v_{\text{maj}}/\sigma_0) = 0.4$ . 3:1 and 4:1 merger remnants have peaks around  $(v_{\text{maj}}/\sigma_0) = 0.6$  and  $0.8$ , respectively. There are indications for a weak secondary peak around  $(v_{\text{maj}}/\sigma_0) = 1$  for 3:1 and 4:1 remnants.

Figure 12 shows the distribution function in the  $(v_{\text{maj}}/\sigma_0)$ - $\epsilon_{\text{eff}}$  plane. The area of slowly rotating boxy ellipticals (filled boxes) is almost completely covered by remnants of 1:1 mergers while 2:1 mergers have rotational properties resembling faster rotating boxy and slowly rotating disky ellipticals. 3:1 and 4:1 remnants are clearly fast rotating, show high ellipticities and can be associated with fast rotating disky ellipticals. Mergers with an increasing mass ratio produce faster rotating ellipticals with higher ellipticities. All simulated data are in good agreement with observations.

However, there is a trend for the simulated remnants to have slightly larger maximum ellipticities than observed. Projections with high ellipticities ( $\epsilon > 0.5$ ) show systematically smaller values for  $v_{\text{maj}}/\sigma_0$  than observed. The effect is strongest for equal-mass merger remnants and is discussed in detail below. This indicates that the simulated systems are more strongly supported by anisotropic velocity dispersions than the observed systems, despite significant rotation for 3:1 and 4:1 remnants. Observed ellipticals with  $(v_{\text{maj}}/\sigma_0) > 1.2$  can not be reproduced as was already reported by Cretton, Naab, Rix, & Burkert (2001).

The minor-axis kinematics of the simulated remnants was measured as the rotation velocity along the minor axis at  $0.5r_{\text{eff}}$ . The amount of minor axis rotation was parametrized as  $(v_{\text{min}}/\sqrt{v_{\text{maj}}^2 + v_{\text{min}}^2})$  (Binney 1985). Minor axis rotation in elliptical galaxies, in addition to isophotal twist, has been suggested as a sign for a triaxial shape of the main body of elliptical galaxies (Wagner, Bender & Moellenhoff 1988; Franx Illingworth & De Zeeuw 1991). Indeed, 1:1 mergers show a significant amount of minor-axis rotation (Figure 13). This is consistent with their mostly triaxial shape and the measured isophotal twist. 3:1 and 4:1 remnants are more oblate and show weak minor axis rotation. However, the amount of isophotal twist is comparable to equal-mass merger remnants. A detailed analysis of the connection between intrinsic shape, isophotal shape, and internal kinematics is beyond the scope of this paper and needs further investigation.

The anisotropy parameter  $(v_{\text{maj}}/\sigma_0)^*$  was defined as the ratio of the observed value of  $(v_{\text{maj}}/\sigma_0)$  and the theoretical value for an isotropic oblate rotator  $(v/\sigma)_{\text{theo}} = \sqrt{\epsilon_{\text{obs}}/(1 - \epsilon_{\text{obs}})}$  with the observed ellipticity  $\epsilon_{\text{obs}}$  (Binney 1978). This parameter has been used by observers as a test whether a given galaxy with observed  $v_{\text{maj}}$ ,  $\sigma_0$  and  $\epsilon_{\text{obs}}$  is flattened by rotation ( $(v_{\text{maj}}/\sigma_0)^* \geq 0.7$ ) or by velocity anisotropy ( $(v_{\text{maj}}/\sigma_0)^* < 0.7$ ) (Davies et al. 1983; Bender 1988; Nieto, Capaccioli & Held 1988; Scorza & Bender 1995).

Figure 14 shows the normalized histograms for the  $(v_{\text{maj}}/\sigma_0)^*$  values of the simulated

remnants. The 1:1 remnants peak around  $(v_{\text{maj}}/\sigma_0)^* \approx 0.3$  with a more prominent tail towards lower values. Only about 10% of the projections have  $(v_{\text{maj}}/\sigma_0)^* > 0.6$ . In contrast 82% have  $(v_{\text{maj}}/\sigma_0)^* < 0.4$  and would clearly be interpreted as being supported by anisotropic velocity dispersion. 2:1 remnants peak at  $(v_{\text{maj}}/\sigma_0)^* \approx 0.5$  with 41% showing  $(v_{\text{maj}}/\sigma_0)^* > 0.6$ . 3:1 and 4:1 mergers with peaks at  $(v_{\text{maj}}/\sigma_0)^* \approx 0.6$  and  $(v_{\text{maj}}/\sigma_0)^* \approx 0.7$  are consistent with model predictions of oblate isotropic or slightly prolate rotators. The percentage of projections with  $(v_{\text{maj}}/\sigma_0)^* > 0.6$  is 64% and 83%, respectively. 3:1 and 4:1 remnants also have predominantly disk-like isophotes and cover the area populated by observed disk-like ellipticals in the  $\log(v_{\text{maj}}/\sigma_0)^* - a_{4\text{eff}}$  diagram (Figure 15).

1:1 merger remnants show the most complex behaviour. A significant number of the projected remnants lie in a region of disk-like anisotropic systems where no elliptical galaxy is observed. Assuming that a projected remnant clearly fails to resemble an observed elliptical if it has  $a_4 > 0.3$  and  $(v_{\text{maj}}/\sigma_0)^* < 0.5$ , 28% of the 1:1 remnants would fall into the forbidden regime.

To understand the behaviour of equal-mass remnants in more detail we illustrate the influence of the initial orientation of the progenitor disks on the properties of the merger remnants. We defined mean values of the investigated quantities of all 500 projections for every merger geometry. Thereafter we divided the equal-mass remnants into four groups of geometries that produce remnants with almost distinct properties: slowly rotating boxy remnants with  $\overline{v_{\text{maj}}/\sigma_0} < 0.2$  and  $\overline{a_4} < -0.4$  (group A; geometries 2,4,5, and 14), slowly rotating remnants with predominantly disk-like isophotes having  $\overline{v_{\text{maj}}/\sigma_0} < 0.2$  and  $\overline{a_4} > 0.25$  (group B; geometries 1,8,9,11, and 13), modestly rotating remnants ( $\overline{v_{\text{maj}}/\sigma_0} > 0.2$ ) that appear to be isotropic with  $(v_{\text{maj}}/\sigma_0)^* > 0.7$  (group C; geometries 7, 12, and 15) and remnants with modest deviations in isophotal shape  $-0.2 < \overline{a_4} < 0.2$  (group D; geometries 3,6,12, and 16). The results are shown in Figure 16.

Remnants of group A are slowly rotating anisotropic systems with purely boxy isophotes. More than 90% of the projected remnants are consistent with observations of boxy anisotropic elliptical galaxies. This class of equal-mass merger remnants was sampled by Naab, Burkert & Hernquist (1999). Most projections of group B show disk-like isophotes and appear to be anisotropic. Around 60% of the projected remnants of this group fail to fall on the observed correlation. Furthermore the remnants of this group show too high ellipticities at low rotation velocities, a behaviour already described by Heyl, Hernquist & Spergel (1996). The shaded regions in Figure 16 indicate the location of the highly elliptical projections ( $\epsilon > 0.4$ ). They dominate the disk-like anisotropic branch of "not observed" merger remnants. It is possible that the very elongated projections of group B would be classified as S0 galaxies. Some of them,

as NGC4550, show weak net rotation and are still very elongated. Geometry 1 produces a very axisymmetric remnant with two counterrotating populations of stars in as it is observed in NGC4550 (see e.g. Pfenniger (1999)). However, Rix, Franx, Fisher, & Illingworth (1992) argued that a merger origin for this particular galaxy is unlikely as it would have heated both disks too much.

Group C combines all rotating 1:1 remnants. They appear slightly diskly or boxy depending on the orientation and are isotropic. It has to be noted that even the diskly remnants of this group are consistent with observations and only 10% of the projections are failures. This group shows a clear connection to the initial conditions as the spins of the progenitor disks were almost aligned. Projections of group D can either have diskly or boxy isophotes and are mostly anisotropic. 35% of the projections fall in the forbidden regime.

#### 4. Conclusions & Discussion

We used a large set of N-body simulations of collisionless mergers of disk galaxies with mass ratios of  $\eta = 1, 2, 3$ , and 4 to investigate for the first time statistical properties of disk-merger remnants. In contrast to previous studies where only projections along the principal axes were investigated we analyzed a large number of randomly projected merger remnants and compared the results in a consistent way to observations. Galaxies on the sky are also viewed along random lines of sight therefore this is the appropriate way of comparison.

We showed that the detailed isophotal and kinematical properties of the simulated merger remnants reach their equilibrium values relatively fast after the merger of the central parts of the galaxies is complete and thereafter do not significantly evolve with time. The high resolution of the simulations made it possible to keep the errors, especially for  $a_4$ , at a reasonably low value and enabled us to perform a statistical analysis.

The basic result is that the projected kinematical and photometric properties of remnants of major mergers of disk galaxies are in surprisingly good agreement with the observational data for elliptical galaxies. The mass ratio of the progenitor disks determines the global properties of the remnants. The influence of the initial orientation on the remnants is strongest for equal-mass mergers.

Purely boxy, anisotropic and slowly rotating remnants with a large amount of minor axis rotation can only be produced by equal-mass mergers with certain initial orientations. However, if the initial spins of the disks were almost aligned the remnants appear to be isotropic and diskly or boxy, depending on the viewing angle. In total 28% of all projected 1:1 remnants show properties that are not observed at all. As some of these remnants

have high ellipticities and very small  $(v_{\text{maj}}/\sigma_0)^*$  they appear to be flattened by strongly anisotropic velocity dispersions. In addition they mostly show very disk-like isophotes. As we can not exclude that mergers with these geometries have occurred they should be observed, which is not the case. If this controversy is not solved in the future it might constitute a serious problem for the merger hypothesis. However, if observed, these elongated disk-like objects might have been classified as S0s and have therefore been excluded from the observed sample of bona fide ellipticals.

Based on the diverse properties of the 1:1 remnants they more likely resemble the class of intermediate mass giant ellipticals in the transition region from rotating disk-like to non-rotating boxy ellipticals. In this regime even boxy rotating galaxies have been observed (Nieto & Bender 1989).

In contrast, 3:1 and 4:1 mergers form a more homogeneous group of remnants. They have preferentially disk-like isophotes, are fast rotating and show small minor axis rotation independent of the assumed projection. In general the properties are in very good agreement with observations of fast rotating disk-like ellipticals.

2:1 mergers have intermediate properties with boxy or disk-like isophotes depending on the projection and the orbital geometry of the merger. Globally, different projection angles and orbits do not change the fundamental properties of 1:1 mergers on the one side and 3:1 and 4:1 mergers on the other side.

In summary, many photometric and kinematical properties of low and intermediate mass giant elliptical galaxies can be understood as a sequence of major mergers of disk galaxies with varying mass ratios. The homogeneous group of massive boxy ellipticals populates the boxy anisotropic area of the  $(v_{\text{maj}}/\sigma_0)^* - a4_{\text{eff}}$  plane. Their distribution is inconsistent with the distribution of simulated 1:1 remnants. Therefore they are most likely not remnants of equal-mass mergers of disk galaxies. Boxy and mildly anisotropic remnants are only reproduced by a small subsample of initial conditions. There is no reason why other geometries should have been avoided. It is more likely that massive boxy ellipticals have formed by other processes like mergers of early type galaxies (Naab & Burkert 2000) or multiple mergers in a group environment (Weil & Hernquist 1996).

The simulations presented here were purely dissipationless, taking into account only the stellar and dark matter component of a galaxy. The importance of gas in galaxy-galaxy mergers and the detailed influence on the structure of elliptical galaxies is not fully understood up to now. Numerical simulations of galaxy mergers including gas by Barnes &

Hernquist (1996) and Barnes (1998) have shown that the presence of gas can change the orbital structure and the shape of the merger remnants. As soon as the gas is driven to the center during the merger the mass concentration seems to be responsible for the destruction of stellar box orbits. This process makes it even more difficult to explain the formation of giant boxy ellipticals by binary disk mergers.

The present study will serve as the basis of a further detailed investigation on the influence of an additional dissipative component. Kormendy & Bender (1996) proposed a revised Hubble sequence with disk-like ellipticals representing the missing link between the Im-Spiral-S0 sequence and boxy ellipticals. They noted that gas infall into the equatorial plane with subsequent star formation could lead to a second disk-like subcomponent. Ellipticals with disks could appear disk-like when seen edge-on and boxy otherwise (Scorza & Bender 1995). Our simulations indeed indicate that a disk-like substructure is responsible for producing disk-like isophotes (see Fig. 6). However, in the present case, the disk is the remnant of the more massive spiral which was not completely destroyed during the minor merger (see also Barnes (1998)). Naab & Burkert (2001) investigated line-of-sight velocity distributions of dissipationless merger remnants and found a velocity profile asymmetry that is opposite to the observed one. They concluded that this disagreement can be solved if ellipticals would contain a second disk-like substructure that most likely formed through gas accretion. The situation is however not completely clear, as another study by Bendo & Barnes (2000) found a good agreement of the observed asymmetries for some cases. Naab & Burkert (2001) have shown that extended gas disks can form as a result of a gas rich unequal-mass merger. Barnes (2002) recently presented a first detailed set of equal-and unequal-mass merger simulations of gas-rich galaxies resulting in the formation of extended gas disks. His simulations demonstrate a very complex dynamical evolution. It has to be investigated how the presence of gas changes the detailed properties of the remnants in detail. In addition, star formation during the merger will influence the stellar kinematics (see e.g. Springel (2000)) and the stellar populations by adding young and probably more metal rich stars. As metal enrichment provides a further strong observational constraint on the formation history of early type galaxies (see e.g. Thomas, Maraston, & Bender (2002)) more simulations, including dissipation, star formation and chemical evolution will now be required in order to understand in detail the role of gas for the formation of elliptical galaxies by mergers.

We thank Ralf Bender and Hans-Walter Rix for helpful comments on the script and the referee, Joshua Barnes, for valuable suggestions that significantly improved the paper. All the simulations presented in this work have been performed on the GRAPE cluster at the Max-Planck-Institute for Astronomy in Heidelberg (MPIA). Thorsten Naab is grateful to the

MPIA for its support.

## REFERENCES

- Aragon-Salamanca, A. , Ellis, R. S., Couch, W. J. & Carter, D. 1993, MNRAS, 262, 764
- Barnes, J. E. 1988, ApJ, 331, 699
- Barnes, J. E. 1992, ApJ, 393, 484
- Barnes, J. E. & Hernquist, L. 1992, ARA&A, 30, 705
- Barnes, J. E. & Hernquist, L. 1996, ApJ, 471, 115
- Barnes, J., Galaxies: interactions and induced star formation: lecture notes 1996 / Saas Fee Advanced Course 26, eds. D. Friedli, L. Martinet, and D. Pfenniger, Springer, 1998
- Barnes, J. E. 2002, MNRAS, 333, 481
- Bender, R. 1988, A&A, 193, L7
- Bender, R. 1988, A&A, 202, L5
- Bender, R., Döbereiner, S., & Möllenhoff, C. 1988, A&AS, 74, 385
- Bender, R., Surma, P., Döbereiner, S., Möllenhoff, C. & Madejsky, R. 1989, A&A, 217, 35
- Dynamics & Interactions of Galaxies , ed. R. Wielen, (Heidelberg: Springer), 232
- Bender, R. & Surma, P. 1992, A&A, 258, 250
- Bender, R., Burstein, D., & Faber, S. M. 1992, ApJ, 399, 462
- Bender, R. 1996, IAU Symp., 171, New Light on Galaxy Evolution, ed. R. Bender & R. L. Davies (Dordrecht: Kluwer), 181
- Bender, R. , Ziegler, B. & Bruzual, G. 1996, ApJ, 463, L51
- Bendo, G. J. & Barnes, J. E. 2000, MNRAS, 316, 315
- Beuing, J., Döbereiner, S., Böhringer, H. & Bender, R. 1999, MNRAS, 302, 209
- Binney, J. 1978, MNRAS, 183, 779
- Binney, J. 1985, MNRAS, 212, 767

- Burkert, A. 1993, *A&A*, 278, 23
- Burkert, A. & Naab, T. 2003, astro-ph/0305076
- Burkert, A. & Naab, T. 2003, astro-ph/0301385
- Bekki, K. & Shioya, Y. 1997, *ApJ*, 478, L17
- Bekki, K. 1998, *ApJ*, 502, L133
- Bower, R. G., Lucey, J. R. & Ellis, R. S. 1992, *MNRAS*, 254, 589
- Bruzual A., G. & Charlot, S. 1993, *ApJ*, 405, 538
- Carlberg, R. G. 1986, *ApJ*, 310, 593
- Cretton, N., Naab, T., Rix, H., & Burkert, A. 2001, *ApJ*, 554, 291
- Davies, R. L., Efstathiou, G., Fall, S. M., Illingworth, G. & Schechter, P. L. 1983, *ApJ*, 266, 41
- Davies, R. L. 1996, *IAU Symp.*, 171, *New Light on Galaxy Evolution*, ed. R. Bender & R. L. Davies (Dordrecht: Kluwer), 37
- Davies, R. L., Sadler, E. M. & Peletier, R. F. 1993, *MNRAS*, 262, 650
- Ellis, R. S., Smail, I., Dressler, A., Couch, W. J., Oemler, A., Jr., Butcher, H. & Sharples, R. M. 1997, *ApJ*, 483, 582
- Faber, S. M., et al. 1997, *AJ*, 114, 1771
- Franx, M. & Illingworth, G. D. 1988, *ApJ*, 327, L55
- Franx, M., Illingworth, G. & De Zeeuw, T. 1991, *ApJ*, 383, 112
- Hernquist, L. 1990, *ApJ*, 356, 359
- Hernquist, L. 1992, *ApJ*, 400, 460
- Hernquist, L. 1993a, *ApJS*, 86, 389
- Hernquist, L. 1993b, *ApJ*, 409, 548
- Hernquist, L., Spergel, D. N. & Heyl, J. S. 1993, *ApJ*, 416, 415
- Heyl, J. S., Hernquist, L. & Spergel, D. N. 1994, *ApJ*, 427, 165



- Heyl, J. S., Hernquist, L. & Spergel, D. N. 1996, ApJ, 463, 69
- Kawai, A., Fukushige, T., Makino, J., & Taiji, M. 2000, PASJ, 52, 659
- Kauffmann, G. 1996, MNRAS, 281, 487
- Kauffmann, G. & Charlot, S. 1998, MNRAS, 297, L23
- Khochfar, S. 2003, Ph.D. Thesis, Universität Heidelberg, Deutschland
- Kormendy, J. & Bender, R. 1996, ApJ, 464, L119
- Lauer, T. R., et al. 1995, AJ, 110, 2622
- Makino, J., Fukushige, T. & Namura, K. 2003, to be submitted to PASJ.
- Mehlert, D., Saglia, R. P., Bender, R. & Wegner, G. 1998, A&A, 332, 33
- Mihos, J. C. & Hernquist, L. 1996, ApJ, 464, 641
- Naab, T. , Burkert, A., & Hernquist, L. 1999, ApJ, 523, L133
- Naab, T. & Burkert, A. 2000, ASP Conf. Ser. 197: Dynamics of Galaxies: from the Early Universe to the Present, 267
- Naab, T. & Burkert, A. 2001, ASP Conf. Ser. 230: Galaxy Disks and Disk Galaxies, 451
- Naab, T. & Burkert, A. 2001, ApJ, 555, L91
- Negroponte, J. & White, S. D. M. 1983, MNRAS, 205, 1009
- Nieto, J. -L., Capaccioli, M. & Held, E. V. 1988, A&A, 195, L1
- Nieto, J.-L. & Bender, R. 1989, A&A, 215, 266
- Pfenniger, D. 1999, IAU Symp. 186: Galaxy Interactions at Low and High Redshift, 186, 157
- Pierce, M. J. & Tully, R. B. 1992, ApJ, 387, 47
- Rix, H. -W. & White, S. D. M. 1990, ApJ, 362, 52
- Rix, H. -W. & White, S. D. M. 1992, MNRAS, 254, 389
- Rix, H., Franx, M., Fisher, D., & Illingworth, G. 1992, ApJ, 400, L5
- Jedrzejewski, R. & Schechter, P. L. 1988, ApJ, 330, L87

- Scorza, C. & Bender, R. 1995, *A&A*, 293, 20
- Searle, L. , Sargent, W. L. W. & Bagnuolo, W. G. 1973, *ApJ*, 179, 427
- Springel, V. 2000, *MNRAS*, 312, 859
- Steinmetz, M. & Buchner, S. 1995, *Galaxies in the young universe*, proceedings of a workshop held at Ringberg Castle, eds. H. Hippelein, K. Meisenheimer & H.-J. Röser, Springer, p. 215
- Thomas, D., Maraston, C., & Bender, R. 2002, *Ap&SS*, 281, 371
- Toomre, A. & Toomre, J. 1972, *ApJ*, 178, 623
- Wagner, S. J., Bender, R. & Moellenhoff, C. 1988, *A&A*, 195, L5
- Walker, I. R., Mihos, J. C. & Hernquist, L. 1996, *ApJ*, 460, 121
- Warren, M. S., & Salmon, J. K. 1996, *ApJ*, 460, 121
- Weil, M. L. & Hernquist, L. 1996, *ApJ*, 460, 101
- Wetzstein, M., Nelson, A., Naab, T., & Burkert, A. 2003, in preparation
- Ziegler, B. L. & Bender, R. 1997, *MNRAS*, 291, 527
- Ziegler, B. L., Saglia, R. P., Bender, R., Belloni, P., Greggio, L. & Seitz, S. 1999, *A&A*, 346, 13

Table 1. Orbital parameters

Geometry <sup>a</sup>	$i_1$	$\omega_1$	$i_2$	$\omega_2$	$r_p$	$r_{\text{sep}}$
1/17	0	0	180	0	2	30
2/18	0	0	71	30	2	30
3/19	0	0	71	-30	2	30
4/20	0	0	71	90	2	30
5/21	-109	-60	180	0	2	30
6/22	-109	-60	71	30	2	30
7/23	-109	-60	71	-30	2	30
8/24	-109	-60	71	90	2	30
9/25	-109	0	180	0	2	30
10/26	-109	0	71	30	2	30
11/27	-109	0	71	-30	2	30
12/28	-109	0	71	90	2	30
13/29	-109	60	180	0	2	30
14/30	-109	60	71	30	2	30
15/31	-109	60	71	-30	2	30
16/32	-109	60	71	90	2	30

<sup>a</sup>For unequal-mass mergers the first number indicates the orientation of the more massive galaxy as  $i_1$  and  $\omega_1$ , the second number indicates the orientation of the more massive galaxy as  $i_2$  and  $\omega_2$ .

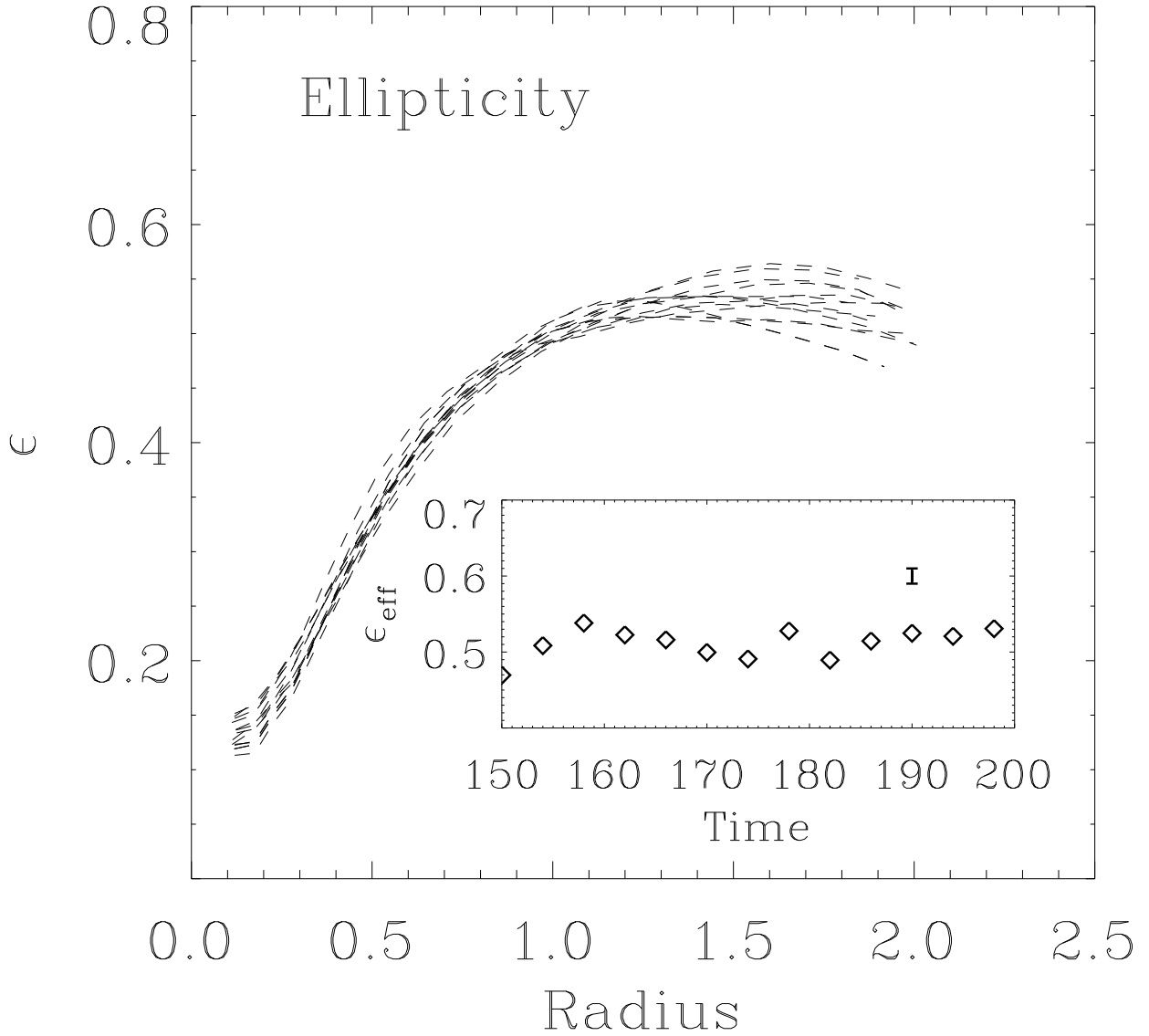


Fig. 1.— Radial change of the ellipticity  $\epsilon$  at different evolutionary times (dashed lines) and the time evolution of the characteristic  $\epsilon_{\text{eff}}$  value for the 3:1 remnant number 10. The error bar for  $\epsilon_{\text{eff}}$  was determined by bootstrapping.

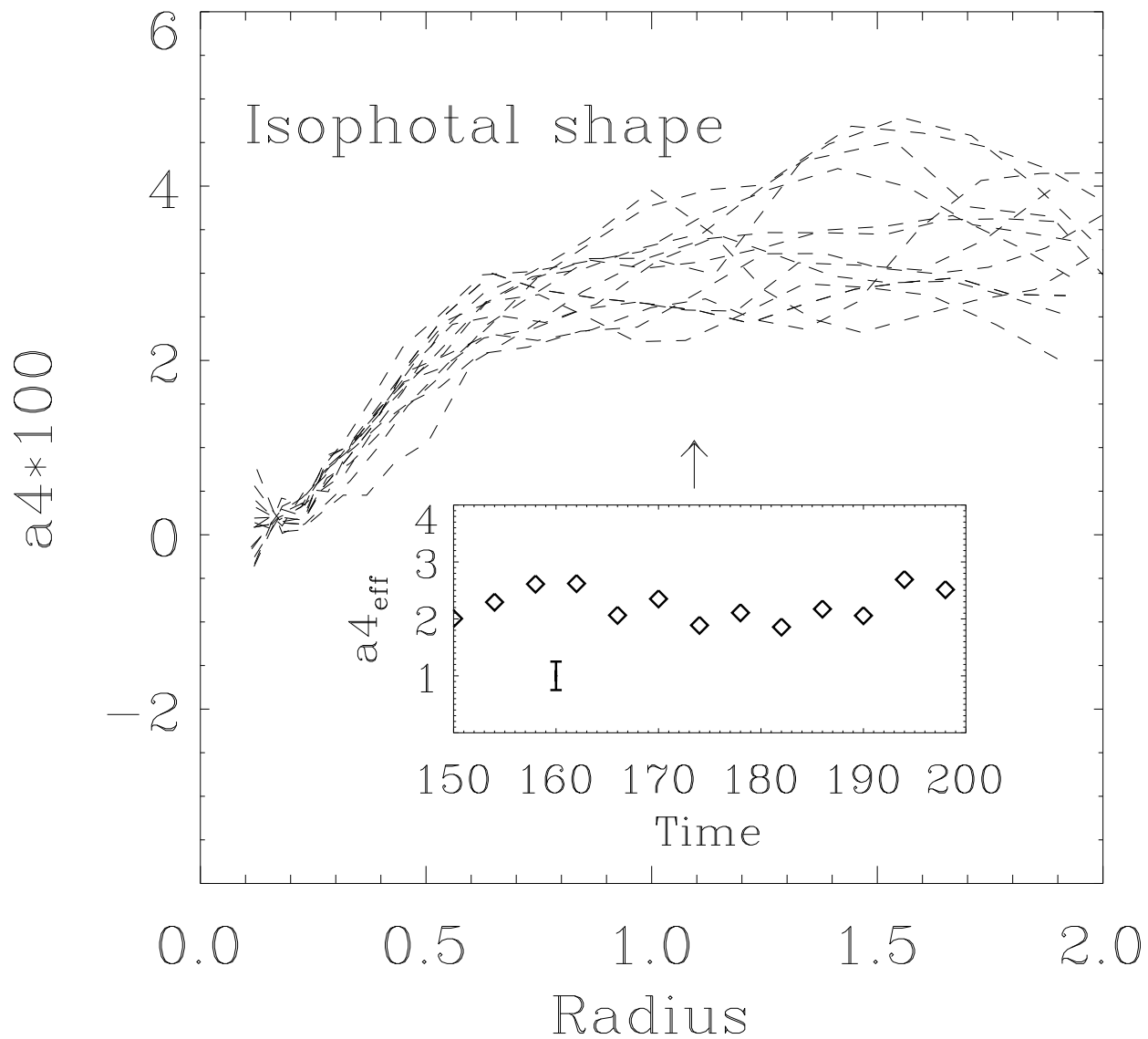


Fig. 2.— Dashed lines show the variation of  $a_4$  along the apparent long axis for different evolutionary times at intervals of  $\Delta t = 10$  for the 3:1 merger remnant 10. The arrow indicates the value of the projected half mass radius  $r_e$ . The small viewgraph shows the time evolution of the effective  $a_{4\text{eff}}$  value assigned to each of the dashed curves. The error bar was determined by statistical bootstrapping.

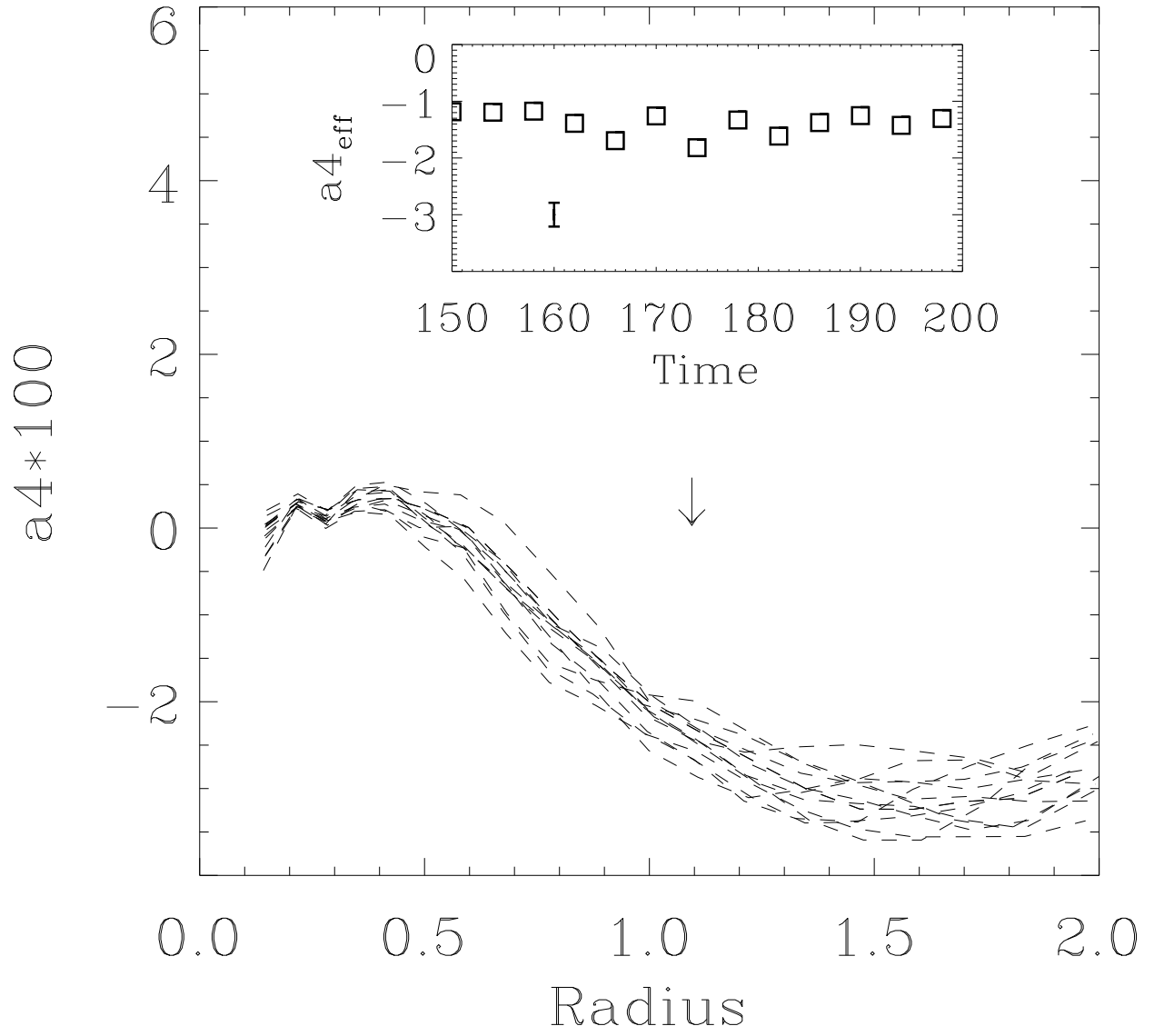


Fig. 3.— Same as Figure 2 but for 1:1 merger remnant 2.

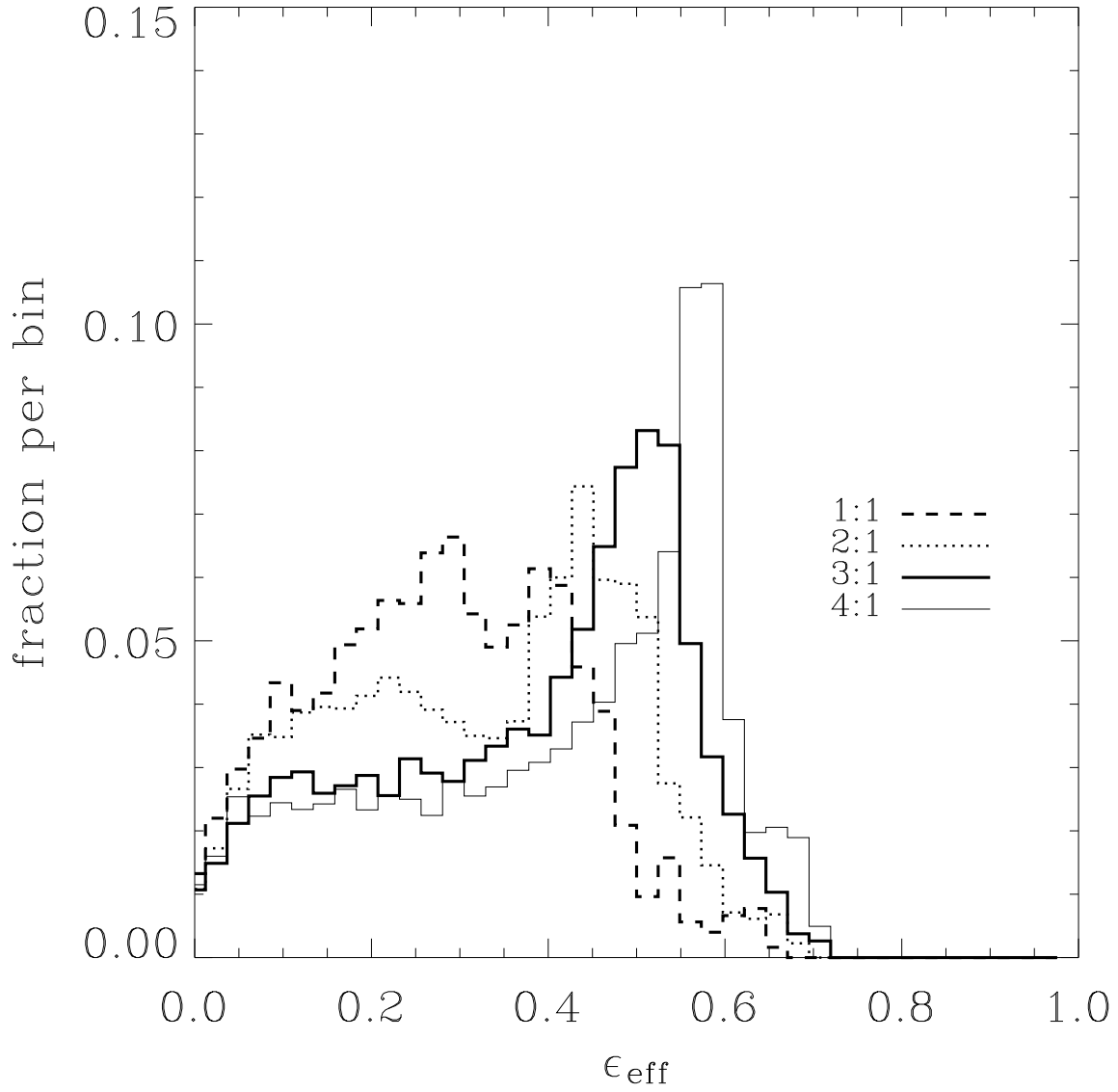


Fig. 4.— Normalized histograms of the effective ellipticity  $\epsilon_{\text{eff}}$  for 1:1, 2:1, 3:1, and 4:1 mergers.

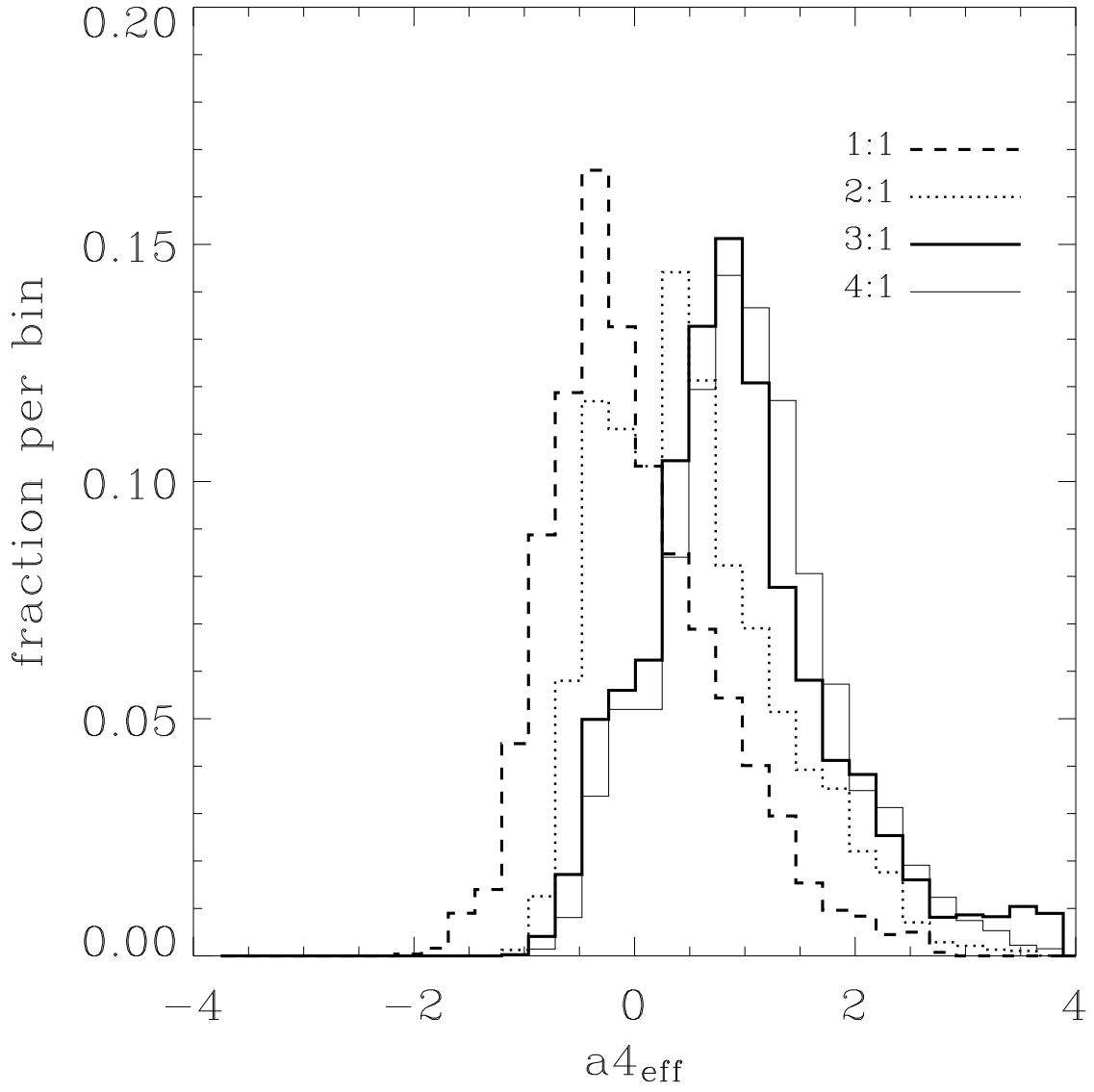


Fig. 5.— Normalized histograms of the shape parameter  $a_{4\text{eff}}$  for 1:1, 2:1, 3:1, and 4:1 mergers.



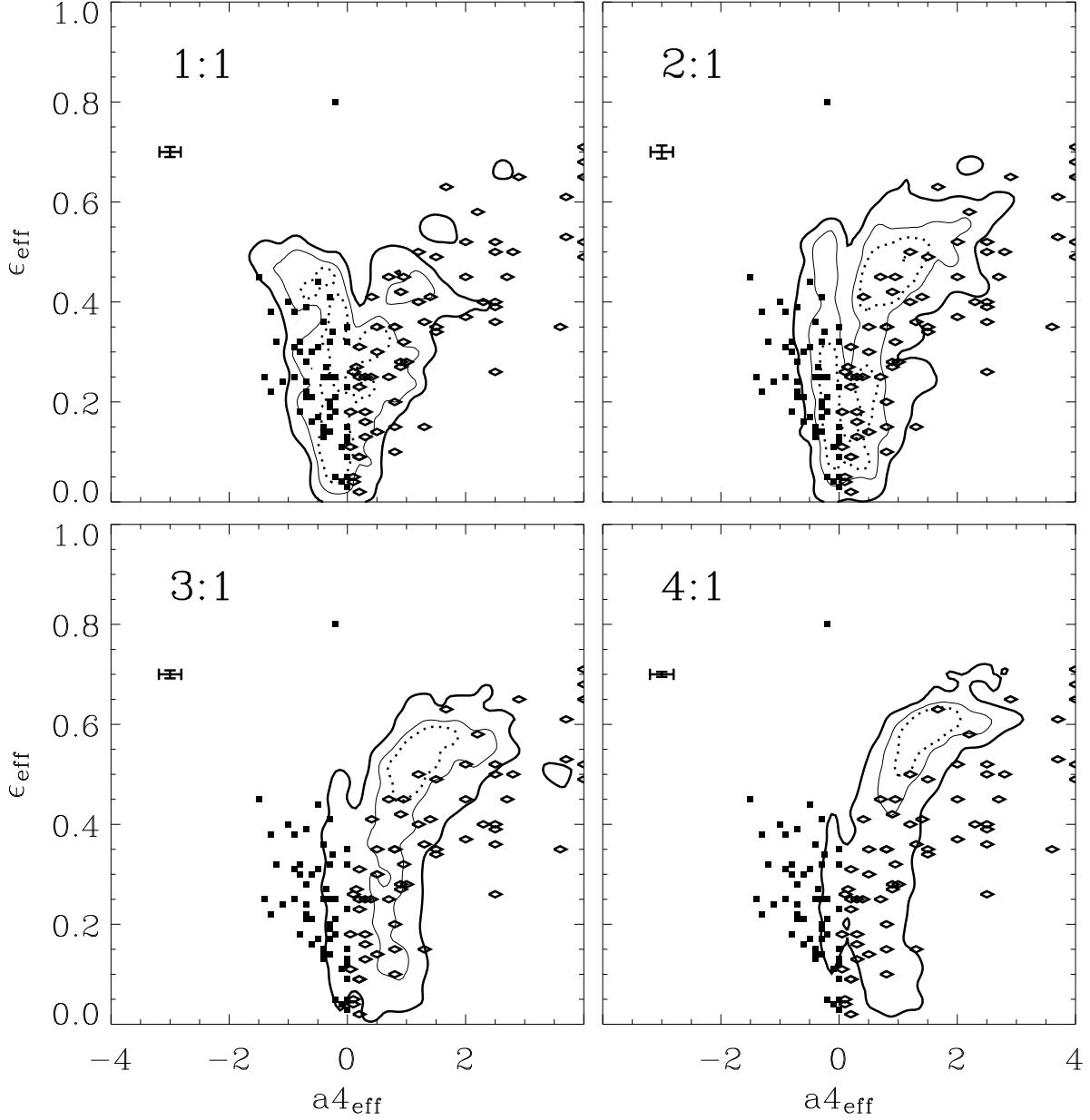


Fig. 6.— Ellipticities  $\epsilon_{\text{ell}}$  versus the characteristic shape parameter  $a_{4\text{eff}}$  for 1:1, 2:1, 3:1, and 4:1 mergers. The contours indicate the 50% (dotted line), the 70% (thin line) and the 90% (thick line) probability to find a merger remnant in the enclosed area. The error bars for  $a_{4\text{eff}}$  are derived applying statistical bootstrapping. Errors for  $\epsilon_{\text{eff}}$  are too small to be visible on this plot. Black boxes indicate values for observed boxy elliptical galaxies, open diamonds show observed disk ellipticals (data from BDM).

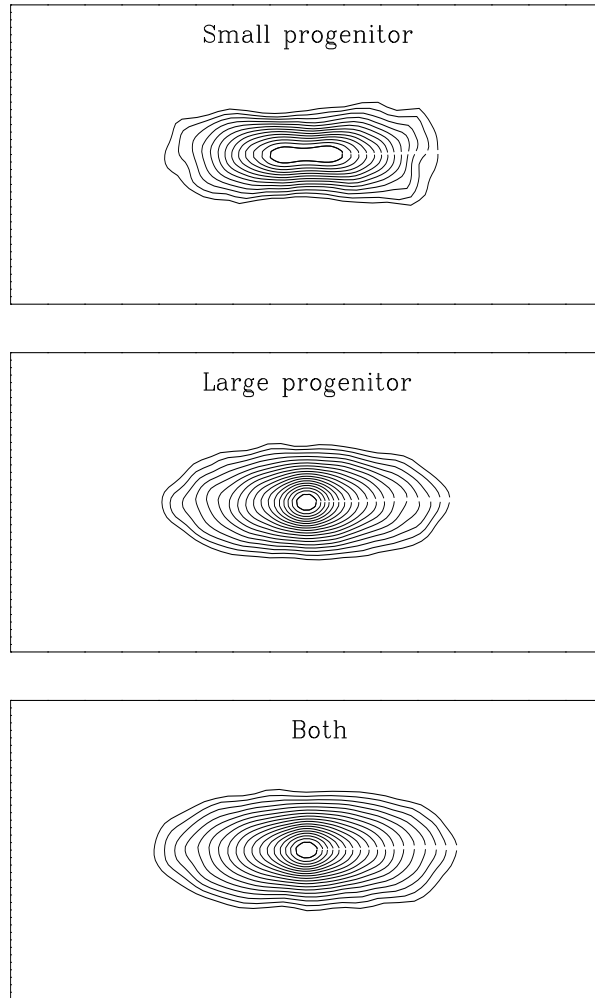


Fig. 7.— Characteristic isodensity contours of a typical 3:1 merger remnant. The two upper panels show the contours for the luminous particles of the smaller and larger progenitor, separately. The lower panel shows the resulting contours of the complete remnant.

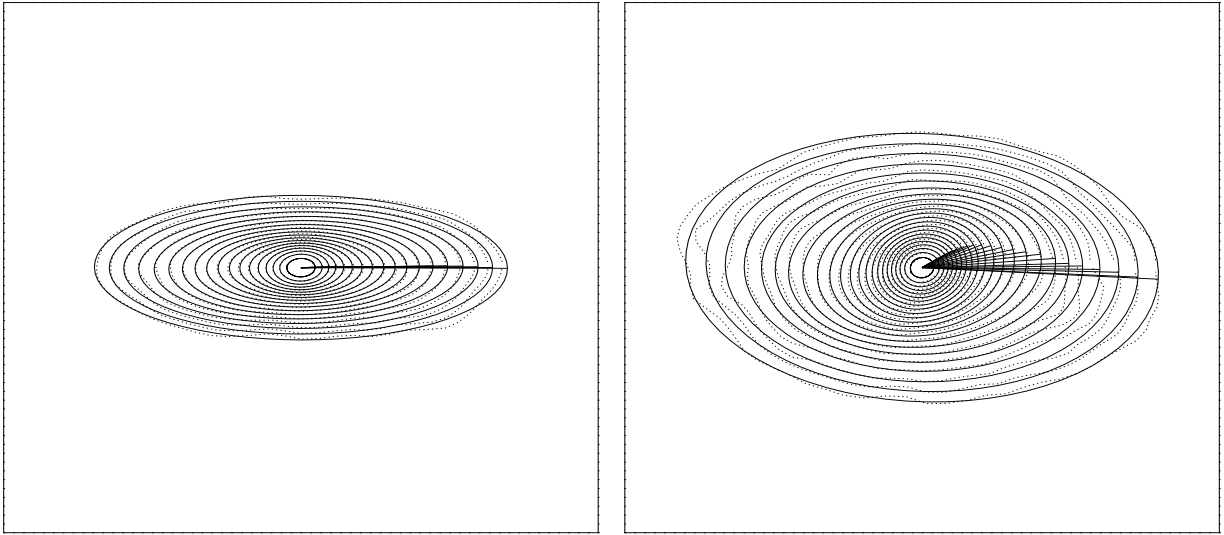


Fig. 8.— The real isophotes (dotted) and the best fitting ellipses (solid line) a typical 3:1 merger remnant seen in a more elongated (left) and rounder (right) projection. The major axes of the fitted ellipses are plotted for every isodensity contour. The change of direction of the axes indicates the isophotal twist. The box length is 3 length units.

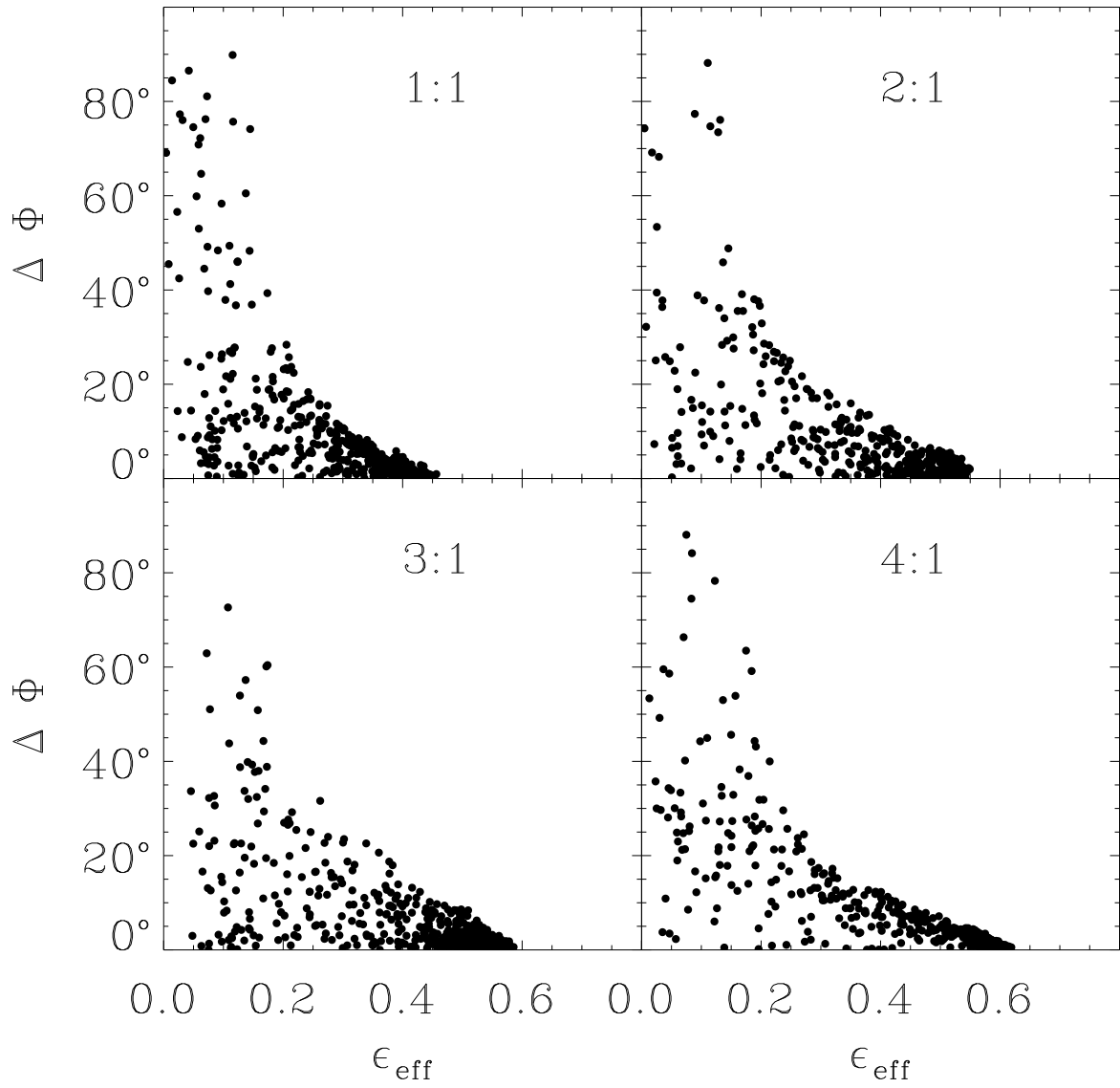


Fig. 9.— Isophotal twists  $\Delta\Phi$  vs. ellipticity  $\epsilon_{\text{eff}}$  for a characteristic 1:1, 2:1, 3:1, and 4:1 merger remnant, respectively. For every mass ratio 500 random projections are shown.

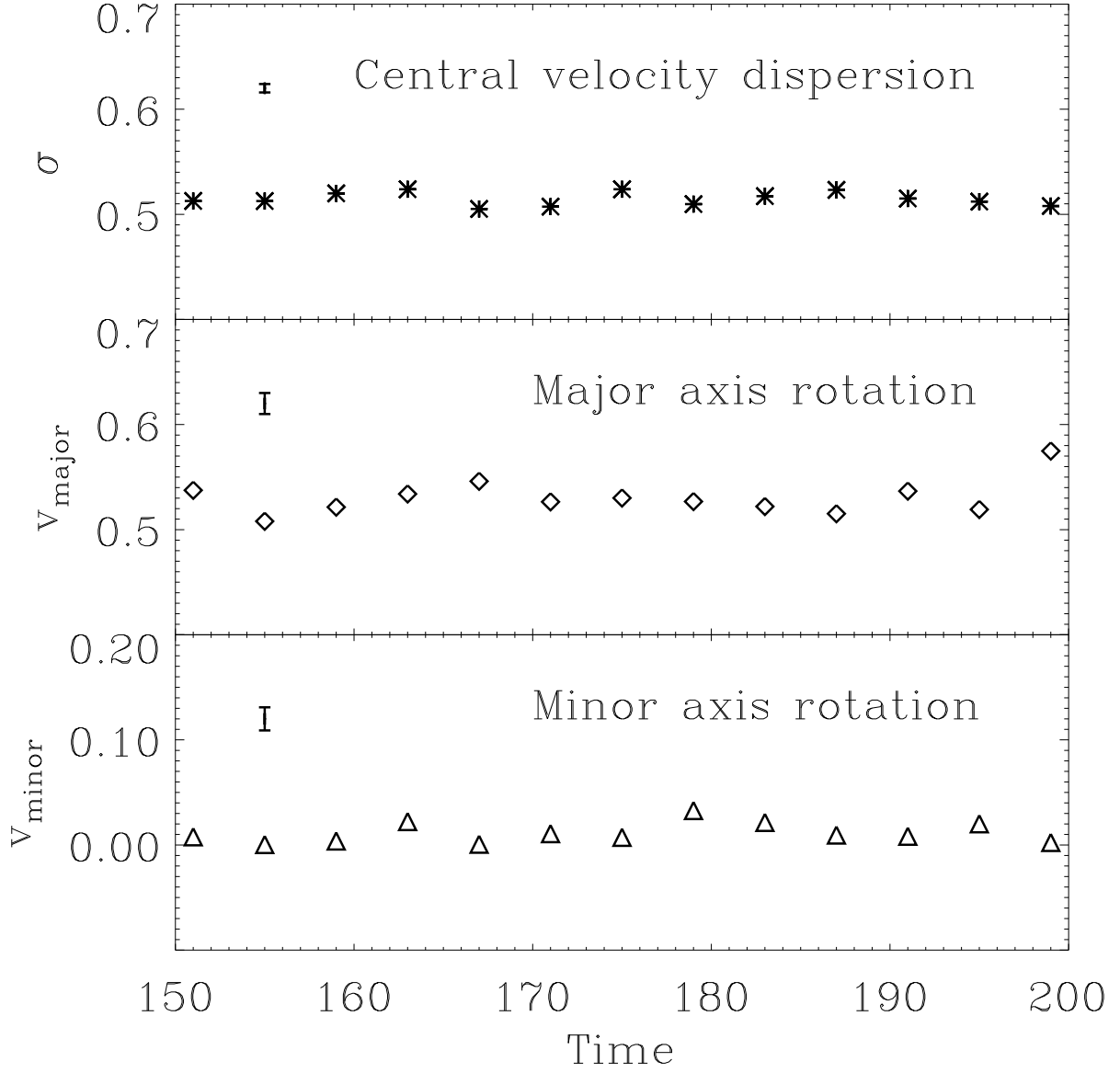


Fig. 10.— Time evolution of the characteristic kinematical parameters for a 3:1 remnant: projected central velocity dispersion  $\sigma$ , major axis rotation velocity  $v_{\text{major}}$  at  $1.5 r_e$ , and minor axis rotation velocity  $v_{\text{minor}}$  at  $0.5 r_e$ . The error bars indicate the bootstrap error.

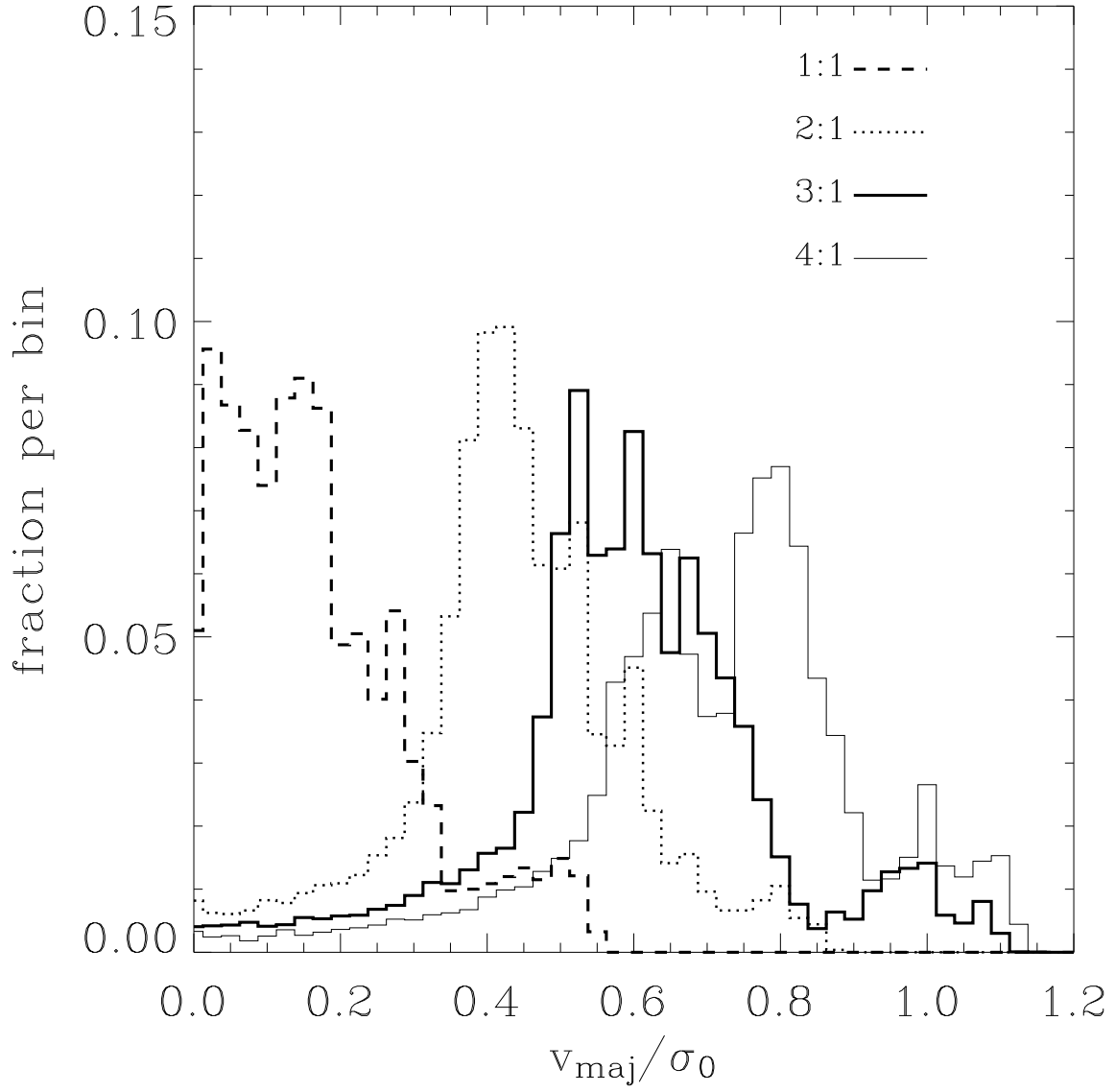


Fig. 11.— Normalized histograms of  $v_{\text{maj}}/\sigma_0$  for 1:1, 2:1, 3:1, and 4:1 mergers.

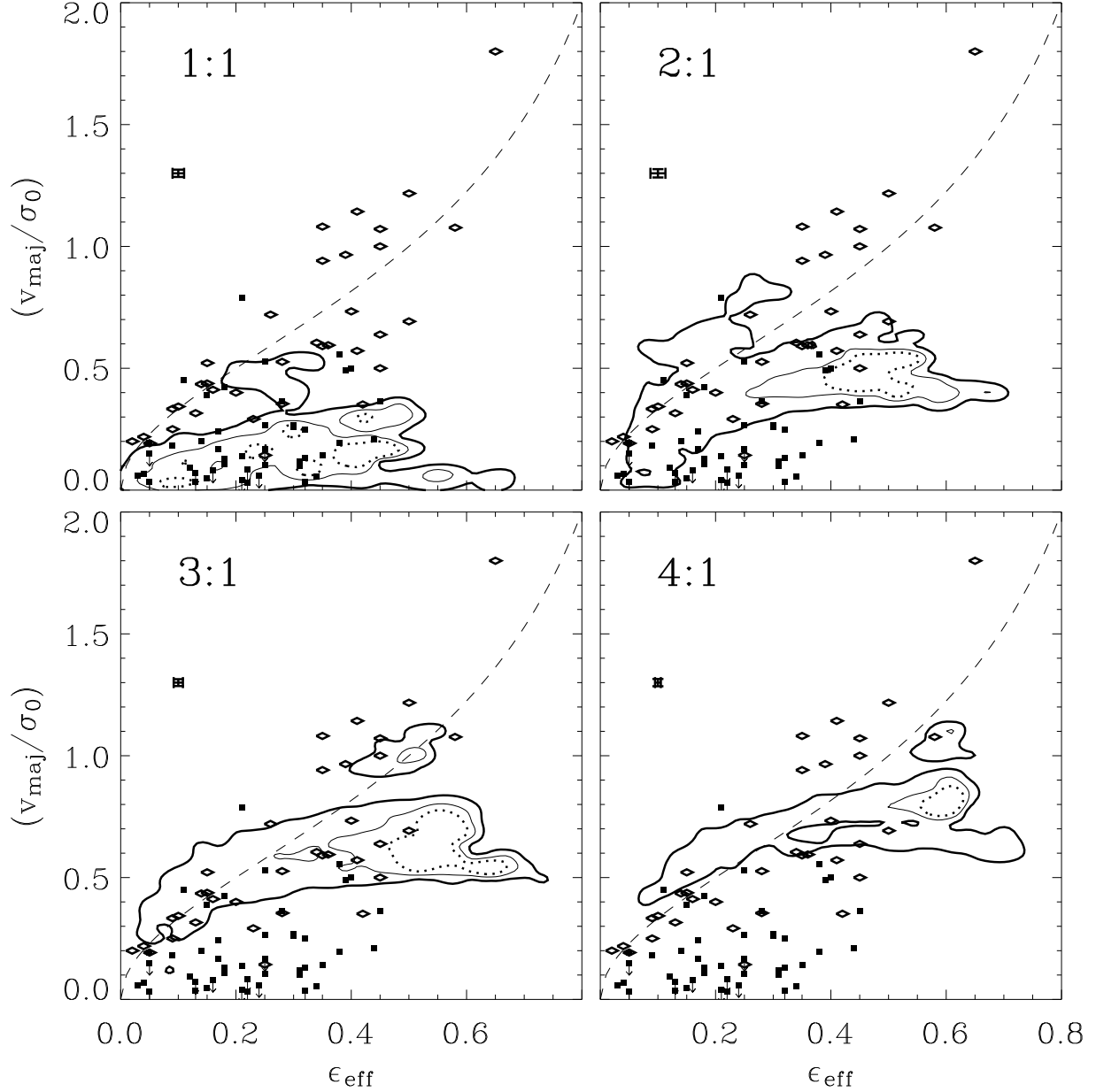


Fig. 12.— Rotational velocity along the major axis  $v_{\text{maj}}$  over the central velocity dispersion  $\sigma_0$  versus the characteristic ellipticity  $\epsilon_{\text{eff}}$  for 1:1, 2:1, 3:1 and 4:1 mergers. The contours indicate the 50% (dotted line), the 70% (thin line) and the 90% (thick line) probability to find a merger remnant in the enclosed area. Values for observed ellipticals are overplotted. Filled boxes indicate data for boxy elliptical galaxies, open diamonds show data for disk ellipticals. Arrows indicate upper limits. The dashed line shows the theoretical value for an oblate isotropic rotator. The error bars were derived by statistical bootstrapping.

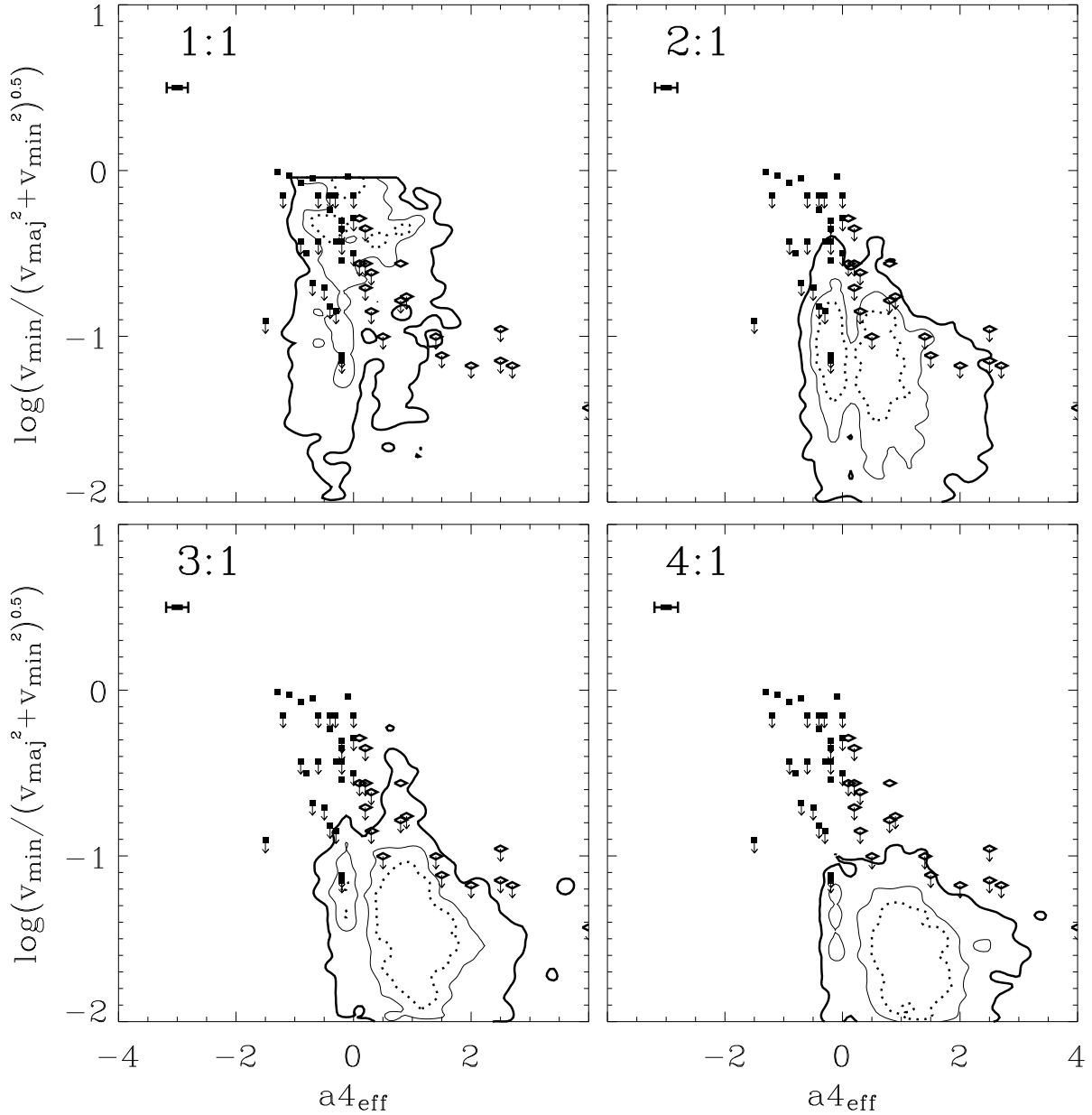


Fig. 13.— Amount of minor axis rotation  $\log(v_{\min}/\sqrt{v_{\text{maj}}^2 + v_{\min}^2})$  versus  $a_{4\text{eff}}$  for 1:1, 2:1, 3:1 and 4:1 mergers. The contours indicate the 50% (dotted line), the 70% (thin line) and the 90% (thick line) probability to find a merger remnant in the enclosed area. Values for observed ellipticals are overplotted. Filled boxes indicate data for boxy elliptical galaxies, open diamonds show data for disk ellipticals. The data with arrows provide an upper limit. The error bars were derived by statistical bootstrapping.



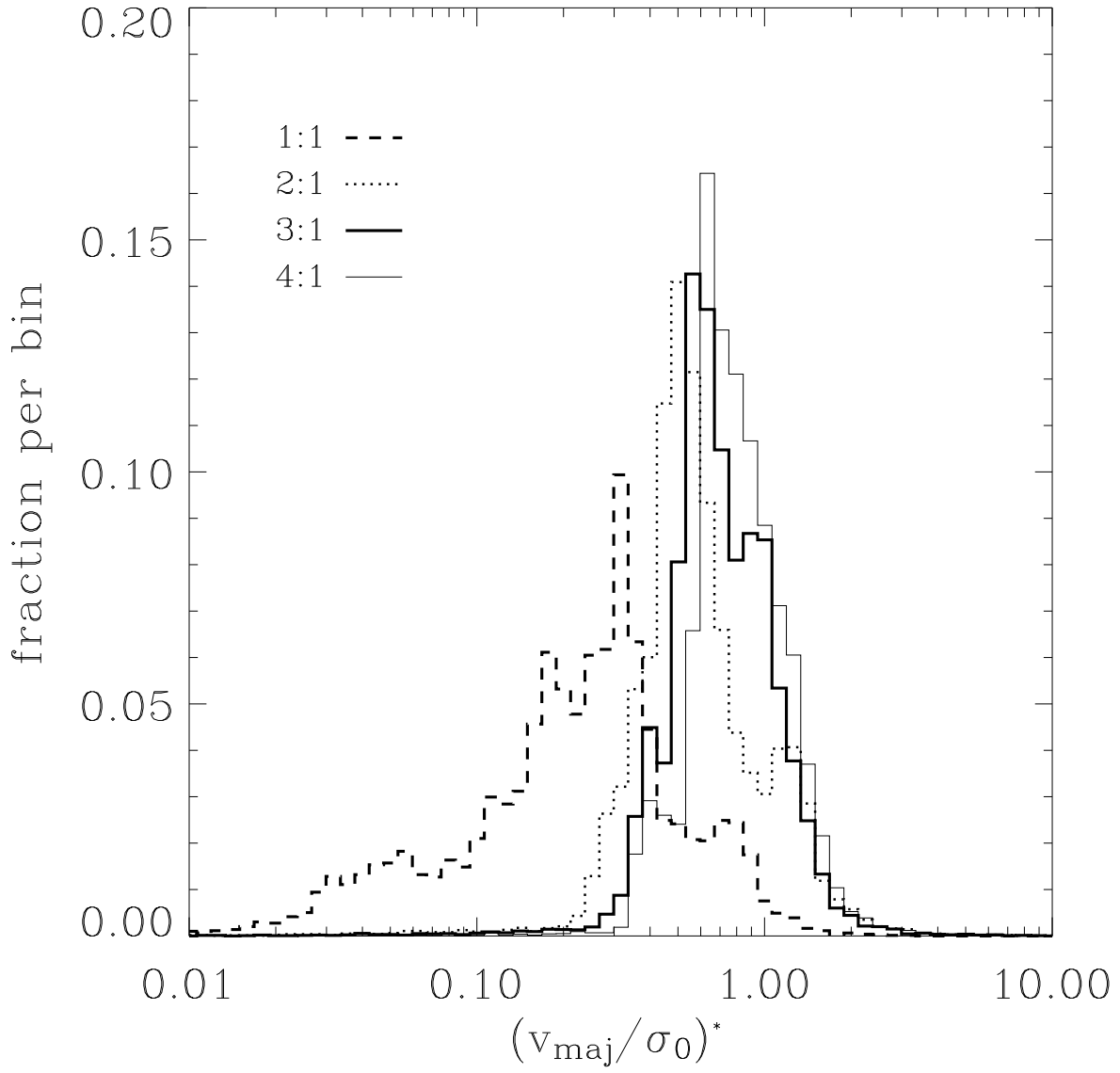


Fig. 14.— Normalized histograms of  $(v_{\text{maj}}/\sigma_0)^*$  for 1:1, 2:1, 3:1, and 4:1 mergers.

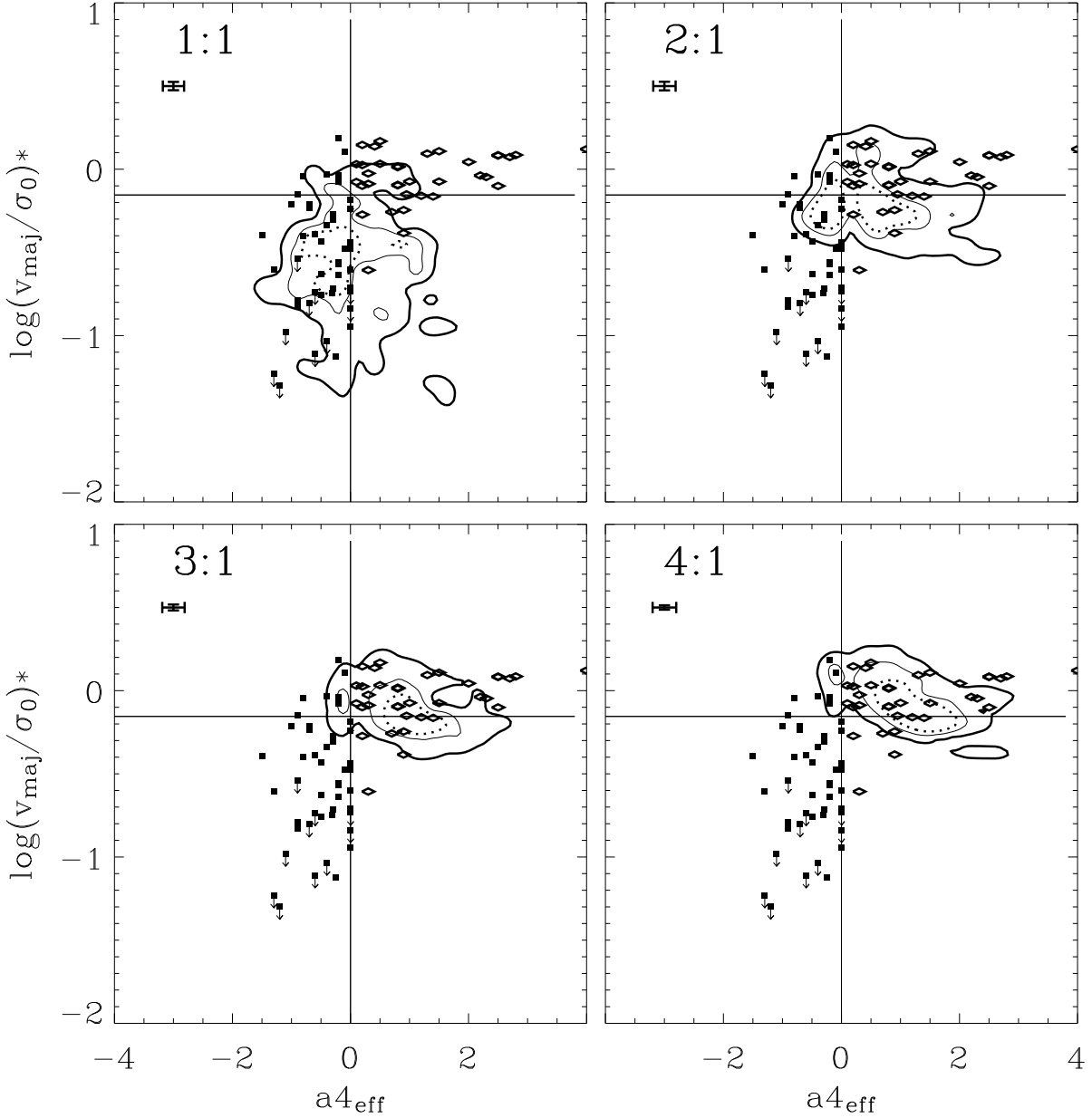


Fig. 15.— Anisotropy parameter  $(v_{\text{maj}}/\sigma_0)^*$  versus  $a_{4\text{eff}}$  for 1:1, 2:1, 3:1 and 4:1 mergers. The contours indicate the 50% (dotted line), the 70% (thin line) and the 90% (thick line) probability to find a merger remnant in the enclosed area. Values for observed ellipticals are overplotted. Filled boxes indicate data for boxy elliptical galaxies, open diamonds show data for disk ellipticals. Arrows indicate upper limits. The error bars were derived by statistical bootstrapping.

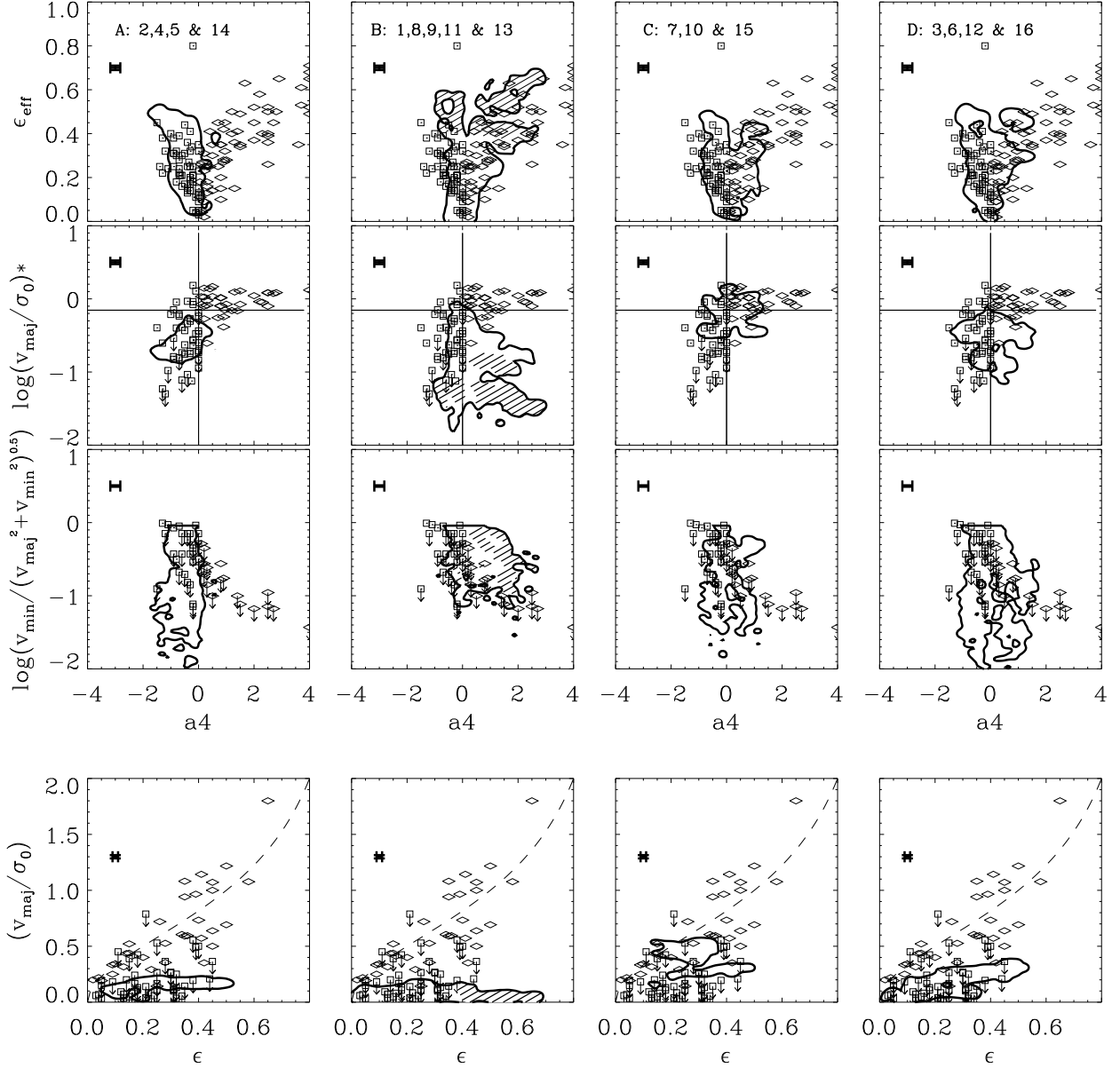


Fig. 16.— Statistical properties of equal-mass merger remnants divided into four groups (A,B,C,and D) according to their average properties (see text). The different initial geometries are given in the first row. The contours indicate the 90% probability to find a projected remnant in the enclosed area. The shaded area in the second column corresponds to the location of projections with ellipticities larger than 0.4.